ELSEVIER

Chemical Geology 239 (2007) 96–123

CHEMICAL GEOLOGY
INCLUDING
ISOTOPE GEOSCIENCE

www.elsevier.com/locate/chemgeo

Eclogitisation of gabbroic rocks: Redistribution of trace elements and Zr in rutile thermometry in an Eo-Alpine subduction zone (Eastern Alps)

C. Miller [a,*], A. Zanetti [b], M. Thöni [c], J. Konzett [a]

[a] *Institut für Mineralogie und Petrographie, University of Innsbruck, Innrain 52, A-6020 Innsbruck, Austria*
[b] *CNR-Istituto di Geoscienze e Georisorse, Unità di Pavia, via Ferrata 1, I-27100 Pavia, Italy*
[c] *Center of Earth Sciences, University of Vienna, Althanstrasse 14, A-1090 Wien, Austria*

Received 20 April 2006; received in revised form 27 December 2006; accepted 2 January 2007

Editor: R.L. Rudnick

Abstract

The investigation of eclogites and a precursor gabbro from the Austroalpine basement domains Koralpe, Saualpe and Pohorje shows that these mafic rocks are similar to oceanic gabbros that were derived from a depleted mantle source. The chemical variations of the eclogites are related to differences in the magmatic history of the precursor rocks and to seawater alteration. The trace element composition of the rocks has not changed significantly during the gabbro to eclogite transformation because trace elements are redistributed among the newly formed high-pressure major and accessory minerals. As other recent studies indicate, incompatible trace elements are predominantly hosted in zoisite/clinozoisite (Sr, Pb, U, Th, LREE), apatite (Sr, Pb, REE), phengite (Cs, Rb, Ba), garnet (Y, HREE, Sc), rutile (Ti, Nb, Ta) and zircon (Zr, Hf) at eclogite-facies conditions. Omphacite hosts most of the Li in addition to some Sr and major amounts of Sc and V. This argues against significant liberation of LILE and LREE during subduction-related dehydration or fluid infiltration of these mafic rocks.

The trace element characteristics of accessory minerals in eclogites help to reconstruct the *P–T–t* evolution of a subduction complex: U–Pb zircon ages will date the high-pressure event if U–Th characteristics and REE analyses constrain zircon growth to being metamorphic and essentially synchronous with the growth of garnet. Recent studies document that variations in Zr content of rutile grown in the presence of zircon and quartz are mainly attributable to differences in temperature. Zr-in-rutile thermometry of Koralpe, Saualpe and Pohorje eclogites yields temperatures of 700–730 °C (according to Zack et al. [Zack, T., Moraes, R., Kronz, A., 2004. Temperature dependence of Zr in rutile: an empirical calibration of a rutile thermometer. Contrib. Mineral. Petrol. 148, 471–488]) or between 630–650 °C (according to Watson et al. [Watson, E.B., Wark, D.A., Thomas, J.B., 2006. Crystallization thermometers for zircon and rutile. Contrib. Mineral. Petrol. 151, 413–433]). No systematic variation in rutile temperatures was observed for matrix rutile and rutile included in garnet, omphacite or kyanite, suggesting that these temperatures represent peak metamorphic conditions and that this part of the Austroalpine basement behaved as a coherent block during subduction.

Keywords: Eastern Alps; Eclogite; Trace elements; Subduction; Rutile thermometry

* Corresponding author.
E-mail address: Christine.Miller@uibk.ac.at (C. Miller).

0009-2541/$ - see front matter © 2007 Elsevier B.V. All rights reserved.
doi:10.1016/j.chemgeo.2007.01.001

1. Introduction

Eclogites are plagioclase-free metamorphic rocks composed of ≥ 75 vol.% of garnet and omphacite (IUGS Subcommission on the Systematics of Metamorphic Rocks). They generally have basaltic bulk compositions and recrystallized at high to ultrahigh pressures during subduction. Trace element and isotopic data of eclogites can be used to identify the geologic settings in which the eclogite precursors formed. In addition, trace element data of eclogites and eclogite minerals are important for assessing recycling processes in subduction zones. Stability or breakdown of mineral phases in a subducting slab influence the composition of aqueous fluids or melts derived from the slab and, hence, the flux of incompatible trace elements into the overlying mantle wedge. The latter, in turn, can explain the distinctive enrichment of large-ion lithophile (LIL) and light-rare earth elements (LREE) relative to high-field strength elements (HFSE) observed in arc magmas (e.g. Maury et al., 1992; Hawkesworth et al., 1993; Tribuzio et al., 1996; Becker et al., 2000; Scambelluri and Philippot, 2001; Zack et al., 2002a; Spandler et al., 2003; John et al., 2004).

This study investigates trace elements, Sm–Nd and Rb–Sr isotopic compositions of gabbros and eclogites from the eclogite type locality in the Eastern Alps (Haüy, 1822) and identifies important trace-element hosting minerals. This information helps to evaluate trace element behaviour of subducting material and to select samples most suitable for dating high/ultrahigh pressure events by means of Sm–Nd and/or Lu–Hf mineral isochrons (e.g.

Table 1
Precision and accuracy determined on BCR-2g and NIST SRM 612 reference materials

	BCR-2					NIST SRM 612				
	Reference value	Measured value (n=24)	S.D. (1σ)	RSD (%)	Accuracy (%)	Reference value	Measured value (n=5)	S.D. (1σ)	RSD (%)	Accuracy (%)
Li (ppm)	9	9	1	11	2	41.54	39.83	1.31	3	4
Sc	33	33	1	3	0.6	41.05	36.23	2.78	8	12
Ti	13,500	13,535	684	5	0.3	–	–	–	–	–
V	416	416	21	5	0.1	39.22	38.10	3.57	9	3
Cr	18	15	2.1	14	15	39.88	36.00	3.24	9	10
Co	37	36.5	2.5	7	1	35.26	32.09	0.92	3	9
Rb	48	48	3.7	8	0.03	31.63	29.90	1.95	7	5
Sr	346	334	18	6	4	76.15	81.67	4.49	5	7
Y	37	34	3	9	8	38.25	39.75	2.30	6	4
Zr	188	184	10	5	2	35.99	35.97	2.23	6	0.07
Nb	13.14(*)	11.5	1.1	10	12	38.06	39.06	1.95	5	3
Cs	1.1	1.1	0.1	9	3	41.64	38.59	1.96	5	7
Ba	683	666	21	3	3	37.74	36.72	2.57	7	3
La	25	26.4	1.1	4	5	35.77	33.76	2.97	9	6
Ce	53	53.0	1.6	3	0.03	38.35	36.61	2.83	8	5
Pr	6.8	6.5	0.2	4	4	37.16	36.80	3.12	8	1
Nd	28	28.1	0.7	3	0	35.24	32.29	2.97	9	8
Sm	6.7	6.5	0.3	5	3	36.72	35.63	4.12	12	3
Eu	2.0	2.0	0.1	5	1	34.44	34.10	3.15	9	1
Gd	6.8	6.4	0.6	9	6	36.95	35.30	3.19	9	4
Tb	1.07	1.04	0.05	5	3	35.92	36.63	3.60	10	2
Dy	6.38(*)	6.19	0.35	6	3	35.97	33.15	3.22	10	8
Ho	1.33	1.32	0.08	6	1	37.87	37.75	3.42	9	0.3
Er	3.66(*)	3.47	0.23	7	5	37.43	35.52	3.44	10	5
Tm	0.54	0.52	0.04	7	4	37.55	36.39	3.33	9	3
Yb	3.5	3.4	0.2	6	2	39.95	36.16	4.52	13	9
Lu	0.51	0.51	0.03	5	0.3	37.71	34.28	4.08	12	9
Hf	4.8	4.8	0.3	6	1	34.77	32.22	3.75	12	7
Ta	0.78(*)	0.68	0.07	11	13	39.77	35.07	4.74	14	12
Pb	11	10.6	0.8	8	4	38.96	32.71	2.34	7	16
Th	6.2	6.1	0.3	5	2	37.23	35.97	3.67	10	3
U	1.69	1.66	0.11	7	1	37.15	35.22	2.39	7	5

Reference values for BCR-2g are taken from USGS web site: (http://minerals.cr.usgs.gov/geochem/basaltbcr2.html), with the exception of the elements marked with * (S.E. Jackson, pers. comm.). Reference values for NIST SRM 612 are taken from Pearce et al. (1997).

Thöni and Jagoutz, 1992; Miller et al., 2005a). As the studied eclogites contain rutile + zircon + quartz, the Zr in rutile thermometers of Zack et al. (2004) and Watson et al. (2006) were tested as alternative methods to the garnet–omphacite Fe^{2+}–Mg exchange thermometers.

2. Analytical procedures

Whole-rock major and trace element analyses were performed through the Service d'Analyses des Roches et des Minéraux du CNRS (SARM) in Nancy. Samples were prepared by fusion in Li metaborate and subsequent dissolution. With the exception of potassium, major elements were determined by ICP-AES, using a Jobin-Yvon JY 70 instrument, trace elements were measured by flow-injection ICP-MS on a Perkin-Elmer ELAN 5000. For calibration and the control of accuracy, international geostandards (Govindaraju, 1994) were used. Detection limits, data precision and accuracy are available at http://www.%20crpg.cnrs-nancy.fr/SARM/sommaire.html. K

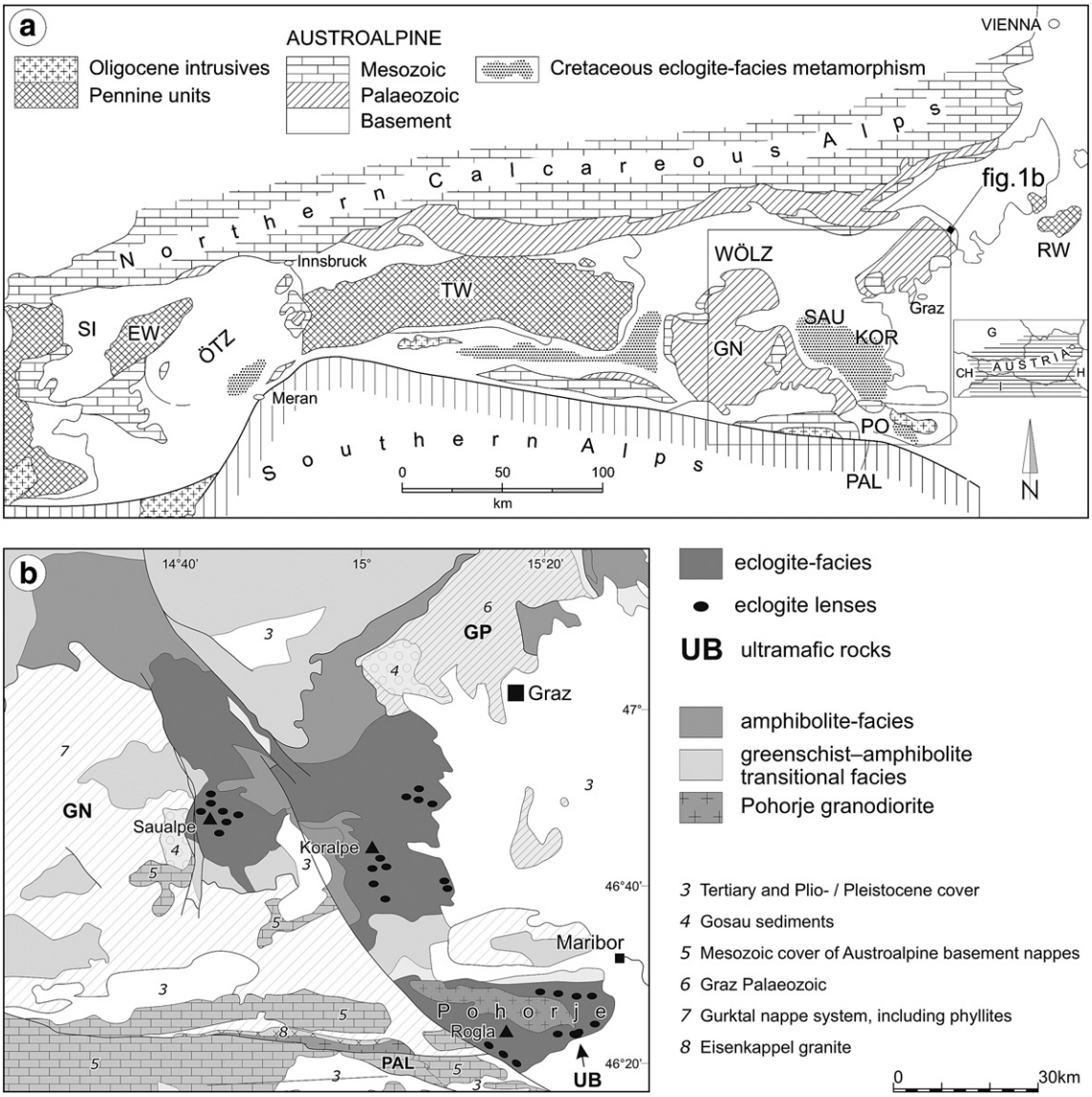

Fig. 1. (a) Simplified geological map of the Eastern Alps, showing Austroalpine basement units and the distribution of Cretaceous eclogite-facies metamorphism (modified from Thöni 2002). PO = Pohorje, KOR = Koralpe, SAU = Saualpe, ÖTZ = Ötztal, SI = Silvretta, GN = Gurktal nappe, TW =Tauern window, EF = Engadine window, RW = Rechnitz window, PAL = Periadriatic lineament. (b) General geology of the easternmost Austroalpine units, including Saualpe, Koralpe and Pohorje high-pressure domains, and major eclogite outcrops. Sample locations are listed in Table 2.

was determined by AAS on a Hitachi Polarized Zeeman AAS Z-8230 at the University of Innsbruck with precision and accuracy better than 1%. The Sm–Nd and Rb–Sr analytical work was performed at the Laboratory of Geochronology, Centre for Earth Sciences, University of Vienna, using thermal ionization mass spectrometry (TIMS). Procedures for sample processing and element separation are described elsewhere (Miller et al., 2005a). Sm, Nd, and Sr were run as metals from an Re double filament, using a Finnigan® MAT262 (for ID) and a ThermoFinnigan® Triton TI TIMS (for IC), while Rb was evaporized using a Ta filament. A $^{143}Nd/^{144}Nd$ ratio of 0.511845 ± 0.000002 ($n=7$) and an $^{87}Sr/^{86}Sr$ ratio of 0.7102491 ± 0.000004 ($n=5$) was determined for the La Jolla (Nd) and the NBS987 (Sr) international standards, respectively, during the period of investigation. Within-run mass fractionation was corrected for $^{146}Nd/^{144}Nd = 0.7219$, and $^{86}Sr/^{88}Sr = 0.1194$, respectively. Concerning Nd isotopes, a continuous depletion of the upper mantle is assumed throughout geological time and the following DM (Depleted Mantle) model parameters were used: $^{147}Sm/^{144}Nd = 0.222$, $^{143}Nd/^{144}Nd = 0.513114$ (Michard et al., 1985).

Mineral analyses were performed on a JEOL JXA-8100 Superprobe (Institut für Mineralogie und Petrographie, University of Innsbruck) using the wavelength-dispersive analytical mode with 15 kV acceleration voltage and a beam current of 10 to 20 nA. For determination of Sr and Ce in epidote-group minerals a beam current of 100 nA and counting times of 100 s on peaks and 50 s on backgrounds were used. Natural and synthetic mineral standards were used. Matrix corrections were performed with a PhiRhoZ routine. For zircon, seven elements (Si, Zr, Hf, Y, P, U, Th) were analysed using 20 kV accelerating voltage and 120 nA beam current with counting times of 120 s on the peak and half that time for background counts for the trace elements. Zr, Nb, Cr, Fe, Al, Si concentrations in rutile were also determined by electron-microprobe, following the method outlined by Zack et al. (2004) with an acceleration voltage of 20 kV and a beam current of 120 nA. As suggested by Zack et al. (2004), Si concentrations were measured to detect beam overlap with adjacent silicates as a quality control. In all cases, measurements were <200 ppm Si and frequently below detection limits (23 ppm). The accuracy of these analyses was checked against rutile standards provided by T. Zack before and after each analytical session.

In situ trace element analyses of individual mineral phases were carried out using laser ablation inductively coupled plasma spectrometry at the CNR-IGG, Unit of Pavia, Italy. The laser probe consists of a Q-switched Nd:YAG laser, model Quantel (Brilliant), whose fundamental emission in the near-IR region (1064 nm) was converted to either 266 nm or 213 nm wavelengths using alternatively two or three harmonic generators (the reader is referred to Jeffries et al. (1998) for the 213 nm wavelength laser configuration). Spot diameter was typically 40–60 μm. The ablated material was analysed by using, alternatively: (i) a double focussing sector-field ICP-MS model Element I (ThermoFinnigan MAT), in which the standard field regulator power stage of the magnet and the ICP torch were upgraded to those of the Element II model; (ii) an Elan DRC-e quadrupole mass spectrometer.

Helium was used as carrier gas and mixed with Ar downstream of the ablation cell. NIST SRM 610 was used as external standard. Ca was used as internal standard for garnet, omphacite, zoisite, amphibole and apatite, Si for phengite and kyanite, Ti for rutile and Zr for zircon. Precision and accuracy were assessed from repeated analyses of the BCR-2g or NIST SRM 612 standards and resulted usually better than 10% (Table 1). Detection limits were typically in the range of 100–500 ppb for Sc, 10–100 ppb for Sr, Zr, Ba, Gd and Pb, 1–10 ppb for Y, Nb, La, Ce, Nd, Sm, Eu, Dy, Er, Yb. Hf and Ta, and usually <1 ppb for Pr, Th and U. A detailed description of instrumental parameters and quantification procedure is given in Tiepolo et al. (2003). Mineral abbreviations follow Kretz (1983).

Table 2
Sample locations and GPS coordinates

Sample	Unit	Coordinates (WGS84)	Altitude (m)
CM15/01–CM20/01	Pohorje	N46°24.82′E15°27.43′	710–720
CM25/01	Pohorje	N46°24.35′E15°31.24′	512
CM41/01	Pohorje	N46°24.60′E15°30.53′	608
RS01/01	Pohorje	N Visole	
CM20/03–CM28/03	Pohorje	N46°25.25′E15°24.22′	960–985
CM31/03	Pohorje	N46°25.25′E15°31.29′	715
CM35/03	Pohorje	N46°24.33′E15°31.21′	530
CM40/03	Pohorje	N46°29.82′E15°06.29′	515
Bär	Koralpe	N46°47.06′E15°05.13′	1180
CM1/04	Koralpe	N46°42.29′E15°05.36′	800
H42	Koralpe	N46°43.32′E15°08.44′	820
KM4	Koralpe	N46°43.96′E15°04.92′	1120
KM10	Koralpe	N46°42.27′E15°06.57′	940
KK1	Koralpe	N46°44.29′E15°00.20′	1660
SKP2	Saualpe	N46°49.53′E14°37.22′	1490
88T35	Saualpe	N46°49.53′E14°37.22′	1520
40T30	Saualpe	N46°49.53′E14°37.22′	1540
SKP12–SKP28	Saualpe	N46°50.04′E14°37.43′	1690
CM11/03	Saualpe	N46°51.21′E14°33.30′	865
SK1, SK12	Saualpe	N46°54.10′E14°35.20′	1279
SJ4	Saualpe	N46°51.56′E14°41.81′	1560
89T63, 89T66	Saualpe	N46°51.93′E14°38.58′	2044

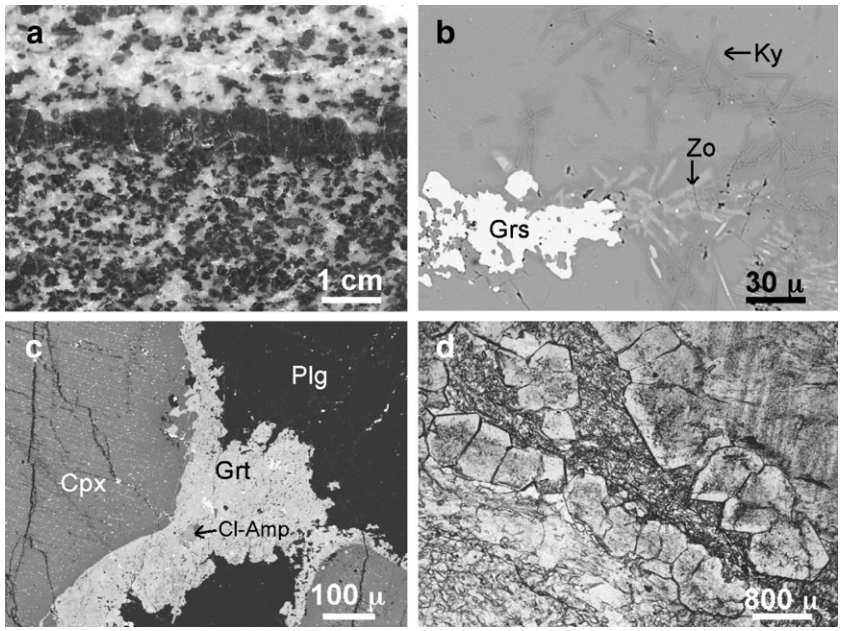

Fig. 2. Examples illustrating the gabbro–eclogite transition at the Bärofen locality, Koralpe. (a) Photograph of an example of igneous layering resulting from different proportions of plagioclase, olivine, clino- and orthopyroxene. (b) BSE image of altered plagioclase domain in a metagabbro sample where calcic plagioclase has partly reacted to grossular-rich garnet, kyanite, zoisite and sodic plagioclase (= slightly darker domains surrounding kyanite and zoisite needles). (c) BSE image of a garnet corona at a clinopyroxene–plagioclase interface in a coronitic metagabbro. Note inclusion of chlorine-rich amphibole in the garnet reaction rim. (d) Photomicrograph of a coronitic Ky-rich eclogite where strings of inclusion-rich garnet separate former pyroxene and plagioclase domains that have reacted to omphacite ± magnesio-hornblende and kyanite + zoisite + quartz, respectively.

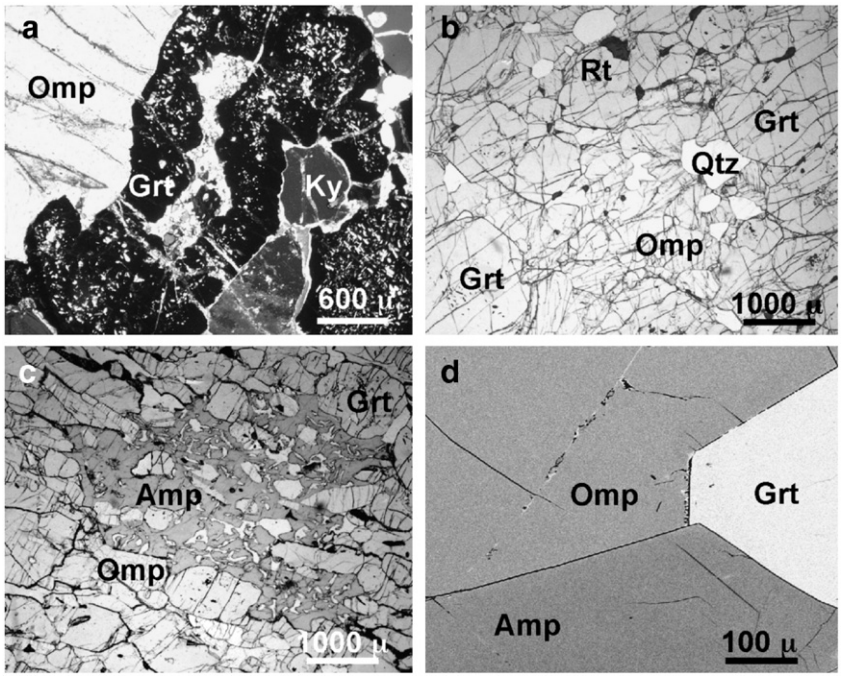

Fig. 3. Photomicrographs and BSE images showing selected micro-textures: (a) high-Mg corona-textured eclogite (CM35/03, Pohorje); (b) low-Mg eclogite (CM11/03, Saualpe); (c) texturally late amphibole poikiloblast (CM1/04, Koralpe); (d) texturally primary magnesio-hornblende (CM31/03, Pohorje). For mineral abbreviations see Kretz (1983).

Table 3
Major (wt.%), trace element (ppm) and isotopic compositions of metagabbros and eclogites from the Koralpe, Saualpe and Pohorje, Eastern Alps

Sample	Bär*	92T06*	94T44*	CM1/04	SK12	SKP23	CM1/03	SKP2	CM11/03	SJ4	CM15/01*	CM41/01	CM27/03	RS01/01	CM35/03
Lithology	Gabbro	Gabbro	High-Mg	Low-Mg	High-Mg	High-Mg	High-Mg	Low-Mg	Low-Mg	Low-Mg	Low-Mg	High-Mg	Low-Mg	High-Mg	High-Mg
Location	K	K	K	K	S	S	S	S	S	S	P	P	P	P	P
SiO_2	48.2	48.1	51.4	49.5	48.1	47.9	50.6	48.7	49.5	50.4	49.1	48.1	48.2	49.3	48.1
TiO_2	0.40	0.29	0.28	1.69	0.42	0.79	0.55	1.67	1.10	1.71	1.77	0.46	1.10	0.21	0.27
Al_2O_3	17.0	20.9	19.9	14.9	20.8	17.2	16.5	14.8	15.3	13.9	14.5	17.3	17.1	20.1	19.1
Fe_2O_3	5.59	4.94	4.47	12.0	5.26	6.89	8.19	13.3	9.79	12.21	12.5	5.50	8.81	3.61	4.31
MnO	0.09	0.08	0.06	0.19	0.09	0.08	0.16	0.23	0.15	0.19	0.18	0.09	0.14	0.04	0.07
MgO	11.7	7.79	6.93	7.57	9.59	8.98	9.05	7.99	8.78	8.25	7.57	11.0	9.47	9.35	11.9
CaO	14.8	14.3	13.9	12.1	15.1	14.8	13.4	11.1	13.2	11.6	11.7	15.1	12.8	12.8	14.7
Na_2O	1.82	1.96	1.47	2.60	1.21	2.51	2.19	2.30	2.43	2.87	2.66	2.05	2.25	3.19	1.62
K_2O	0.02	0.02	0.01	0.04	0.03	0.02	0.01	0.03	0.04	0.05	0.11	0.02	0.03	0.01	0.01
P_2O_5	0.03	0.08	0.02	0.26	0.05	0.13	0.07	0.21	0.10	0.13	0.22	0.08	0.11	0.06	0.02
LOI	0.18	0.27	0.73	−0.40	0.12	0.69	0.08	−0.50	−0.21	−0.50	−0.38	0.30	0.01	0.25	0.2
Total	99.9	98.8	99.1	100.3	100.8	99.9	100.8	99.9	100.2	100.8	100.0	100.0	100.1	98.9	100.2
Mg#	81	76	75	56	78	72	69	54	64	57	54	80	68	84	85
Sc	47	41	30	n.d.	18	44	n.d.	45	n.d.	n.d.	46	34	n.d.	n.d.	n.d.
V	160	110	119	304	95	214	222	327	249	353	325	160	214	101	101
Cr	897	420	784	212	448	368	317	183	224	191	180	557	552	1076	1270
Co	32	28	25	40	30	34	33	48	39	42	44	37	39	25	28
Ni	154	106	104	66	159	100	86	63	78	61	68	193	131	228	230
Cu	63	85	64	33	29	27	45	62	19	36	57	46	45	19	50
Zn	30	27	26	76	10	59	58	113	48	88	67	30	65	41	25
Ga	13	14	14	18	16	17	15	19	16	18	18	12	15	14	11
Rb	0.97	0.75	0.72	0.69	0.70	0.82	0.78	<bdl	1.15	<bdl	0.97	1.2	2.59	<bdl	0.69
Sr	83	107	80	99	271	180	140	47	141	50	64	116	123	25	44
Y	8	6	6	36	12	19	15	40	21	36	37	7	21	3.0	5

(continued on next page)

Table 3 (*continued*)

Sample	Bär*	92T06*	94T44*	CM1/04	SK12	SKP23	CM1/03	SKP2	CM11/03	SJ4	CM15/01*	CM41/01	CM27/03	RS01/01	CM35/03
Lithology	Gabbro	Gabbro	High-Mg	Low-Mg	High-Mg	High-Mg	High-Mg	Low-Mg	Low-Mg	Low-Mg	Low-Mg	High-Mg	Low-Mg	High-Mg	High-Mg
Location	K	K	K	K	S	S	S	S	S	S	P	P	P	P	P
Zr	21	16	13	87	35	45	17	111	69	118	107	20.0	54	25	11.2
Nb	1.10	0.90	1.0	2.18	1.40	1.41	0.50	2.18	1.90	1.90	2.10	0.71	2.13	0.30	0.50
Ba	18	26	31	<bdl	12	4.8	6.4	<bdl	4.5	<bdl	9	9.1	9.8	5.60	7
U	0.04	0.03	n.d.	0.10	0.08	0.26	0.03	0.16	0.30	0.13	0.29	0.03	0.23	<bdl	0.03
Pb	1.10	0.98	n.d.	4.20	1.21	9.20	4.98	3.17	12.0	1.87	1.15	1.31	5.86	1.40	0.97
Hf	0.54	0.33	n.d.	2.47	0.92	1.38	0.58	2.69	1.91	3.17	2.98	0.48	1.57	0.68	0.38
Ta	0.11	0.06	n.d.	0.19	0.08	0.12	0.04	0.19	0.11	0.16	0.20	0.04	0.17	0.03	0.03
Th	0.05	0.02	0.20	0.15	0.06	0.10	0.06	0.16	0.08	0.18	0.18	0.02	0.30	<bdl	0.02
La	0.64	0.53	0.60	4.01	0.84	1.65	1.42	3.03	2.04	3.95	3.33	0.37	4.74	0.23	0.35
Ce	2.03	1.51	1.80	12.4	2.44	5.25	4.51	10.4	6.58	13.3	10.5	1.13	13.0	0.30	1.07
Pr	0.35	0.27	0.30	2.17	0.46	0.90	0.79	1.67	1.17	2.38	1.82	0.21	2.06	0.12	0.20
Nd	2.04	1.38	1.56	11.8	2.65	4.88	4.31	8.76	6.51	13.0	10.5	1.25	10.7	0.62	1.14
Sm	0.82	0.57	0.59	4.23	1.18	1.76	1.60	3.20	2.45	4.36	3.42	0.57	3.20	0.32	0.42
Eu	0.45	0.46	0.49	1.62	0.69	0.72	0.67	1.24	0.97	1.55	1.28	0.39	1.11	0.15	0.18
Gd	1.11	0.76	0.81	5.72	1.60	2.55	2.21	4.95	3.34	5.31	4.98	0.96	3.44	0.52	0.65
Tb	0.23	0.15	0.16	0.98	0.29	0.42	0.39	0.90	0.58	0.91	0.90	0.16	0.56	0.09	0.12
Dy	1.48	1.03	1.05	6.20	1.89	2.80	2.50	6.09	3.74	5.97	6.13	1.15	3.59	0.56	0.88
Ho	0.32	0.22	0.21	1.28	0.41	0.63	0.52	1.33	0.77	1.27	1.35	0.25	0.75	0.12	0.19
Er	0.91	0.61	0.62	3.66	1.18	1.82	1.50	3.65	2.20	3.68	3.79	0.71	2.21	0.32	0.57
Tm	0.13	0.09	0.09	0.55	0.18	0.29	0.23	0.59	0.33	0.55	0.61	0.11	0.33	0.05	0.09
Yb	0.80	0.56	0.55	3.62	1.21	1.90	1.51	3.70	2.22	3.70	4.01	0.72	2.21	0.36	0.58
Lu	0.11	0.08	0.08	0.55	0.18	0.29	0.24	0.55	0.35	0.57	0.59	0.11	0.34	0.06	0.09
$^{143}Nd/^{144}Nd$	0.513147	0.513103	0.513112	0.513086			0.513096	0.513067	0.513107		0.513055	0.513141	0.513011		
$^{87}Sr/^{86}Sr(i)$	0.7025	0.7029	0.7025	0.7042			0.70362	0.7071	0.70563		0.70464	0.70292	0.70528		
$\varepsilon(t)^{Nd}$	8.4	7.4	7.6	8.1			8.1	8.0	8.2		8.0	7.4	7.8		

*Analyses published elsewhere; <bdl = below detection limit; n.d. = not determined.

K_2O determined by AAS, Sc determined by ICP-OES.

Initial Sr and Nd isdotope values calculated for a protolith age of 250 Ma.

3. Geological setting

The Koralpe–Saualpe–Pohorje domain forms the south-eastern-most part of the Austroalpine basement units, north of the Periadriatic lineament (Fig. 1) (Table 2). It is characterized by an intense Cretaceous ("Eo-Alpine") high-pressure (HP) metamorphic overprint. Numerous eclogite lenses are now embedded within a sequence of quartz schists, mafic layers and meta-carbonates. Phase equilibria and isotopic constraints on both eclogites and garnet–mica–schists indicate peak pressure conditions of around 2.2–2.5 GPa and 700–750 °C approximately 90 Ma ago (Thöni and Jagoutz, 1992; Thöni and Miller, 1996; Miller and Thöni, 1997; Miller et al., 2005a,b). These eclogites are derived from Permian MORB-type gabbroic protoliths generated in a rift zone that could have been connected with a marginal oceanic basin (Thöni and Jagoutz, 1992; Janák et al., 2004). Subduction of the attenuated passive Tethys margin caused by the convergence of Apulia and Europe started in Jurassic time, inducing closure of the Meliata basin and deep intracontinental subduction of considerable parts of the northern part of Apulia (the Austroalpine basement), including the Permian rift zone rocks. These rocks are now exposed in the Koralpe–Saualpe–Pohorje domain of the "Eo-Alpine HP belt" (Sölva et al., 2005), a more or less coherent zone of eclogite-facies rocks that crop out along an E–W trending zone in the Austroalpine basement units over nearly 400 km along strike of the Alpine chain. (Fig. 1). Sample locations are given in Table 2.

4. Petrology

At the Bärofen and Gressenberg localities in the Koralpe, the transition from medium- to coarse-grained oxide-poor gabbro, gabbro–norite and olivine gabbro to eclogite can be studied *in situ.* The gabbros display numerous crystal–plastic and brittle deformation features, including foliated and ultramylonitic fabrics. Modal layering is locally present (Fig. 2a). The coronitic stage of the gabbro–eclogite transformation is characterized by the breakdown of olivine to complex aggregates consisting of orthopyroxene, green spinel± clinopyroxene+garnet±corundum. Igneous orthopyroxene has narrow coronas of sodic augite when in contact with plagioclase. Breakdown of plagioclase (Fig. 2b) starts at grain boundaries and in high-strain domains within grains with the growth of tiny kyanite± zoisite needles and grossular-rich garnet (Grs_{53-91}). Plagioclase composition becomes more sodic as reactions proceed, suggesting that kyanite and zoisite nucleated at an early stage of plagioclase decomposition, probably by the continuous reaction [Pl+H_2O=Ky+Zo+Qtz+$(NaSiCa_{-1}Al_{-1})_{Pl}$] that proceeds to the right with increasing pressure (Goldsmith, 1982). Clinopyroxene reacts with plagioclase forming garnet coronas along grain boundaries (Fig. 2c). This corona garnet is strongly zoned with higher values of grossular (Grs_{75-81}) and inclusions of kyanite±zoisite towards plagioclase, and lower grossular (Grs_{35-38}) and inclusions of rutile towards clinopyroxene. In addition, inclusions of pargasitic amphiboles containing up to 3.3 wt.% Cl in the garnet reaction rims (Fig. 2c) document the presence of Cl-bearing fluids at the onset of HP metamorphism. The final breakdown of the igneous minerals and formation of eclogite must involve complex net transfer reactions and extensive material transport between different chemical domains. Eclogites that still preserve igneous textures show string-like clusters of garnet separating former plagioclase and mafic mineral domains (Fig. 2d). Plagioclase is replaced by kyanite±zoisite±quartz, pyroxene and olivine are replaced by omphacite+quartz±magnesio-hornblende+rutile. As already pointed out by Ahrens and Schubert (1975a,b), the presence of an intergranular fluid is a pre-requisite for the gabbro–eclogite transformation at $T<600$–800 °C. The presence of zoisite and magnesio-hornblende in the coronitic eclogites clearly documents involvement of a fluid. As discussed e.g. by Mork (1985) and John and Schenk (2003), fluid-controlled dissolution, transport and precipitation processes control the gabbro-to-eclogite transformation. Because most Koralpe, Saualpe and Pohorje eclogites are foliated, ductile deformation may have enhanced reaction kinetics as well.

The studied eclogites are texturally well equilibrated and contain garnet, omphacite, quartz, kyanite, zoisite/clinozoisite, rutile, apatite, zircon±phengite, calcic–subcalcic amphiboles, paragonite (as inclusion in garnet), dolomite, chalcopyrite and pyrite (Miller, 1990; Janák et al., 2004; Sassi et al., 2004). Amphiboles may be in textural equilibrium with omphacite and garnet, but more frequently form anhedral porphyroblasts overgrowing the foliation defined by omphacite±zoisite±kyanite± phengite (Fig. 3). Veins oriented subparallel to the foliation and filled with coarse-grained quartz, kyanite, zoisite±omphacite document the presence of a fluid phase during HP metamorphism. Retrogression is documented by narrow symplectites of Na-poor clinopyroxene, calcic amphibole and sodic plagioclase around omphacite. Kyanite, too, is surrounded by complex symplectites consisting of corundum+anorthite±spinel±

sapphirine±Mg-staurolite, and phengite is replaced by a biotite+plagioclase symplectite.

Krogh Ravna and Terry (2004) and Brandelik and Massonne (2004) have formulated sets of internally consistent geothermobarometric expressions for reactions between garnet–clinopyroxene–kyanite–phengite–quartz/coesite where net transfer reactions involving the end-members grossular, diopside, muscovite, celadonite, kyanite, quartz/coesite define equilibrium pressure and temperature for kyanite–phengite–quartz/coesite-bearing eclogites. The resulting invariant points for the Koralpe, Saualpe and Pohorje eclogites

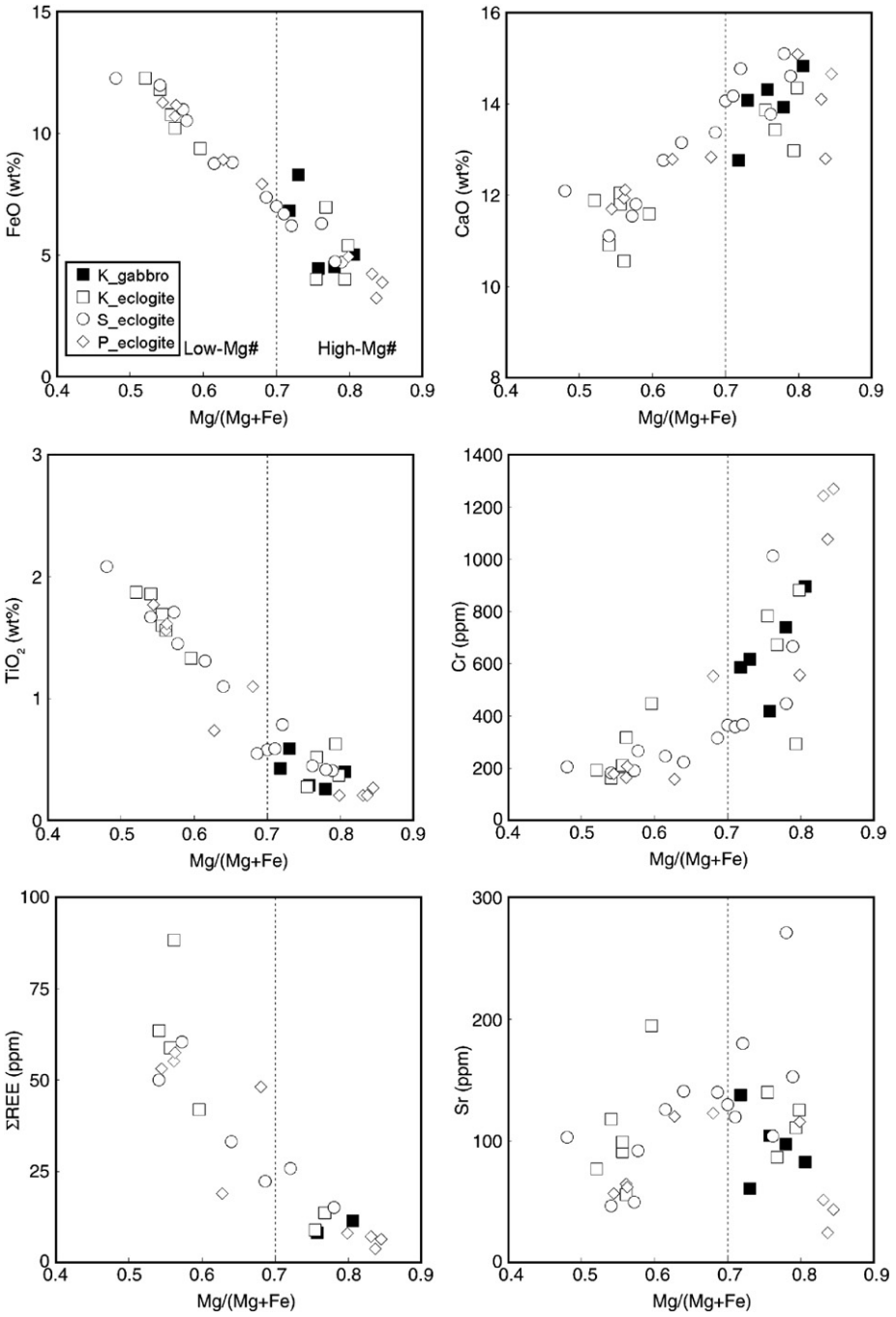

Fig. 4. Plots of selected major and trace elements with Mg-number as differentiation index for Koralpe, Saualpe and Pohorje gabbros and eclogites. Data include analyses published by Miller et al. (1988), Miller and Thöni (1997) and Sassi et al. (2004). See text for discussion.

(Miller and Konzett, 2005) range from 2.2 to 2.4 GPa at 670–760 °C when calculated according to Brandelik and Massonne (2004), and from 2.4 to 2.8 at 700–785 °C when using Krogh Ravna and Terry (2004). Somewhat lower peak pressure estimates of 1.9–2.1 GPa are obtained from phengite-bearing Saualpe and Pohorje eclogites, based on the updated barometer version of Waters and Martin (1993) and corresponding garnet–clinopyroxene temperatures of 630–670 °C obtained with the Krogh Ravna (2000) calibration. In contrast, Janák et al. (2004) suggest a UHP origin for the Pohorje eclogites.

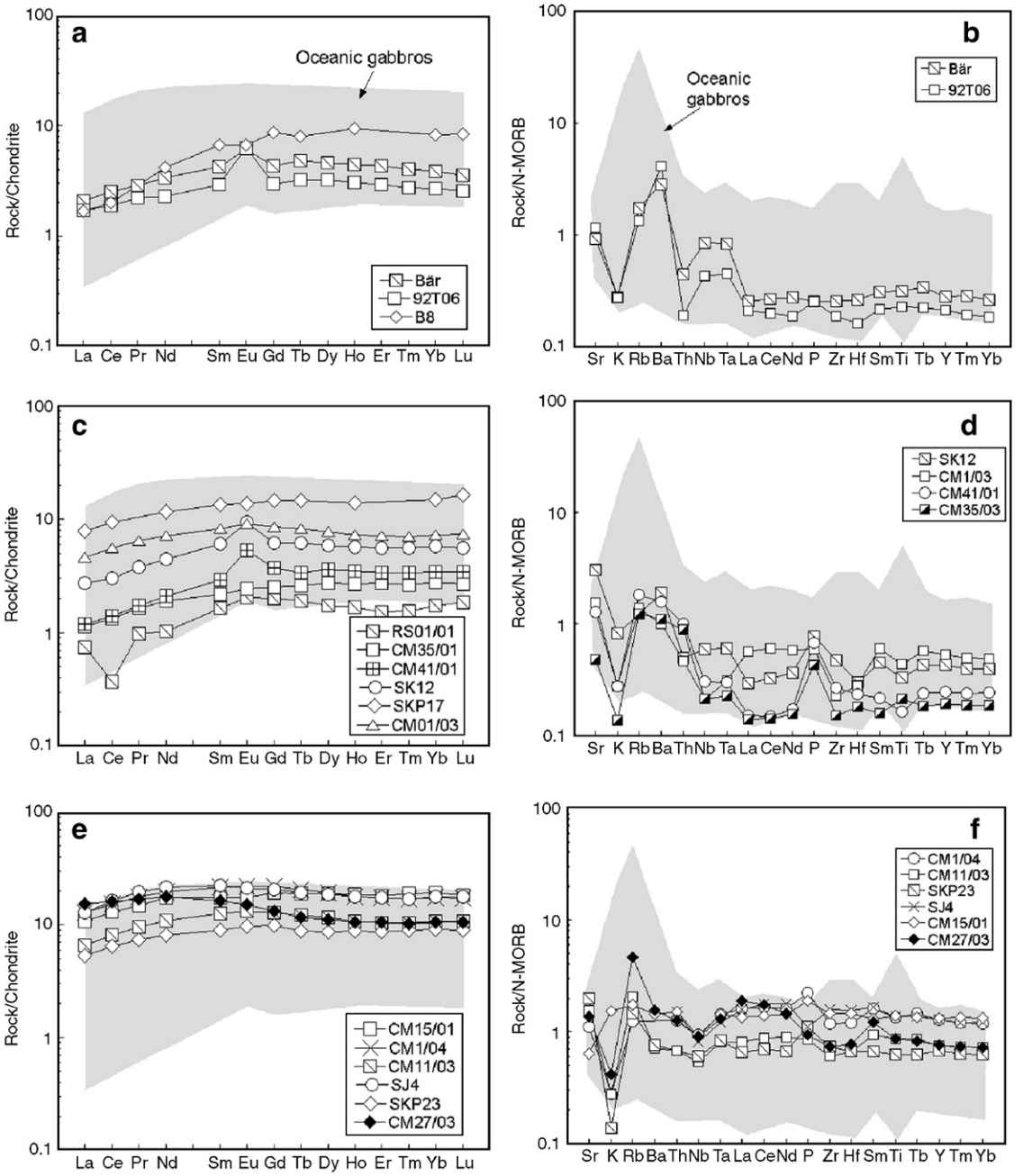

Fig. 5. Chondrite-normalized (Boynton, 1984) REE and N-MORB-normalized (Sun and McDonough, 1989) trace element patterns for (a–b) Koralpe gabbros; (c–d) high-Mg and (e–f) low-Mg Koralpe, Saualpe and Pohorje eclogites compared with a range of oceanic gabbros (shaded field) from MAR and EPR (Ross and Elthon, 1997; Constantin, 1999; Foulger et al., 2005; http://www-odp.tamu.edu).

5. Whole-rock geochemistry

Whole-rock major and trace element analyses of the studied Koralpe metagabbros and Koralpe–Saualpe–Pohorje eclogites are presented in Table 3. Metagabbros and eclogites are rich in Al_2O_3 and CaO and low in alkalis, particularly K_2O. The low-K and trace element characteristics indicate a tholeiitic affinity for all investigated samples. SiO_2 contents show little variation, ranging from 48 to 51 wt.%. Mg-numbers (Mg#=100 Mg/(Mg+∑Fe)) range from 54 to 85, suggesting a cumulate origin for some samples. The data illustrated in Fig. 4 show that compatible elements such as Cr and Ni decrease with decreasing bulk rock Mg# whereas incompatible elements such as Ti and REE increase. This suggests that some of the observed variation reflects igneous differentiation, whereas scattering elemental concentrations such as Rb and Sr may result from redistribution during secondary processes. The gabbros and eclogites derived from early-stage cumulates are characterized by high Mg# (70–85), high CaO (14.3–15.1 wt.%) and low TiO_2 (0.27–0.8 wt.%) contents (Fig. 4). They also have very low abundances of incompatible trace element contents (Fig. 5a–d) and high abundances of Cr (320–1270 ppm). The vertical scatter of Cr in the high-Mg# gabbros and eclogites (Fig. 4) probably reflects presence or absence of Cr-spinel and/or variable incorporation of Cr in pyroxene of the eclogite precusor rocks. The eclogites characterized by Mg# ranging from 54 to 68 have lower Cr, but higher TiO_2 and incompatible trace element contents (Figs. 4, 5e–f). This suggests that the low-Mg eclogites represent non-cumulate gabbros crystallized from more evolved magmas. Kyanite is present in Al-rich compositions of both eclogite types, although modally much more abundant in high-Mg eclogites thought to be derived from plagioclase-rich cumulates. The primary chemical heterogeneities also control variations in mineral compositions. Thus, high-Mg eclogites are often kyanite- and zoisite-rich and characterized by Mg-rich omphacite and garnet compositions, and by omphacite with lower jadeite contents compared with low-Mg eclogites.

Table 4
Trace element data of minerals from Koralpe gabbro

ppm	Plg 1.1	Plg 3.4	Cpx 2.2c	Cpx 2.3r
Li	<bdl	<bdl	1.4	1.5
Sc	1.3	1.2	104	99
Ti	42	305	3477	4197
V	0.02	1.5	416	417
Cr	1	2	1574	1710
Co	0.35	<bdl	45	47
Rb	0.58	0.04	n.d.	n.d.
Sr	258	219	6.6	6.7
Y	0.13	0.20	23	22
Zr	<bdl	0.02	17	19
Nb	<bdl	0.00	0.08	0.11
Ba	4.19	3.15	<bdl	0.07
La	0.56	0.47	0.27	0.28
Ce	1.21	1.07	1.73	1.71
Pr	0.13	0.13	0.49	0.47
Nd	0.52	0.49	3.54	3.52
Sm	0.08	0.10	1.82	1.72
Eu	0.38	0.42	0.61	0.57
Gd	0.04	0.04	2.90	2.88
Tb	0.01	0.01	0.57	0.54
Dy	0.03	0.04	3.74	3.58
Ho	0.01	<bdl	0.84	0.82
Er	0.01	0.02	2.40	2.24
Tm	<bdl	0.00	0.32	0.32
Yb	0.01	0.01	2.21	2.09
Lu	<bdl	<bdl	0.30	0.29
Hf	<bdl	<bdl	0.58	0.64
Ta	<bdl	<bdl	0.01	0.01
Pb	0.34	0.23	n.d.	n.d.
Th	<bdl	<bdl	0.02	0.02
U	<bdl	<bdl	<bdl	0.01

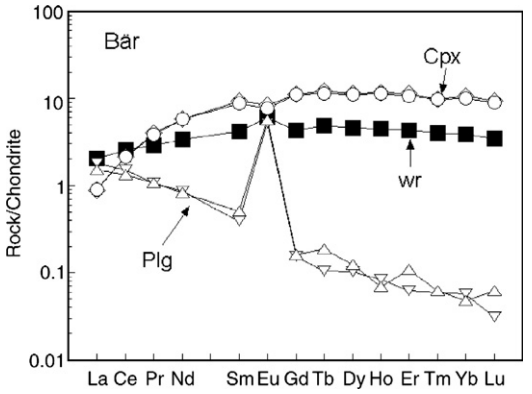

Fig. 6. Chondrite-normalized (Boynton, 1984) REE abundances in minerals and whole rock of an eclogite precursor gabbro from the Koralpe.

Most analysed metagabbros and eclogites are light rare earth element (REE)-depleted with La_N/Yb_N ranging from 0.20 to 0.82 (Fig. 5). The metagabbros and high-Mg eclogites have very low REE abundances consistent with a cumulate origin (Fig. 5a–c). In addition, they frequently display positive Eu anomalies (Eu/Eu*=1.2–2.1) that are a geochemical characteristic of plagioclase-rich cumulates. In contrast, the low-Mg eclogites have flat profiles ranging from 5 to 20 times chondrite (Fig. 5e), sometimes with small negative Eu anomalies (Eu/Eu*=0.87–0.9) suggesting plagioclase fractionation.

New Nd–Sr isotopic data for Koralpe–Saualpe–Pohorje eclogites (Table 3) are within the range reported by Thöni and Jagoutz (1992), Miller and Thöni (1997) and Miller et al. (2005a). Initial εNd values, recalculated

Table 5
Trace element data (ppm) of eclogite minerals determined by LA-ICP-MS

	Garnet					Omphacite					Zoisite/clinozoisite*				
Sample	P_CM15/01	S_SKP2	K_KM10	P_CM41/01	S_SK	P_CM15/01	S_SKP2	K_KM10	P_CM41/01	S_SK	P_CM15/01*	S_CM11/03*	P_CM1/04*	P_CM41/01	S_SK
Lithology	Low-Mg	Low-Mg	Low-Mg	High-Mg	Ky-rich	Low-Mg	Low-Mg	Low-Mg	High-Mg	High-Mg	Low-Mg	Low-Mg	Low-Mg	High-Mg	High-Mg
No. of analyses	(6)	(4)	(2)	(4)	(4)	(6)	(4)	(5)	(4)	(4)	(3)	(1)	(3)	(2)	(1)
Li	0.53	n.d.	0.55	<bdl	0.05	8.6	n.d.	86	15	16	<bdl	<bdl	<bdl	<bdl	<bdl
Sc	65	61	55	76	70	31	34	58	33	46	36	7.84	6.82	7.04	16
Ti	288	300	308.75	139	289	890	867	989	638	905	1079	360	360	360	300
V	106	106	115	29	38	534	585	567	232	244	550	266	257	153	138
Cr	163	168	123	848	1028	68	203	82	690	1294	137	129	160	429	1108
Co	75	75	47	63	59	32	32	28	20	21	2.4	0.85	0.91	0.56	<bdl
Rb	<bdl	n.d.	0.015	<bdl	<bdl	<bdl	n.d.	<bdl	<bdl	<bdl	<bdl	<bdl	<bdl	<bdl	<bdl
Sr	0.06	0.10	0.085	0.04	0.02	69.2	64	14.1	24.9	8.1	1151	2015	1813	939	356
Y	88.4	71.9	119.0	17.4	28.5	1.10	1.48	1.17	0.72	0.85	23.9	48.1	23.2	20.8	44.5
Zr	5.25	4.10	1.95	1.70	6.10	7.13	7.23	7.88	4.61	7.90	15.2	1.61	1.41	1.59	1.54
Nb	<bdl	<bdl	<bdl	<bdl	<bdl	0.007	0.003	0.004	0.009	0.007	<bdl	0.007	<bdl	<bdl	0.01
Cs	<bdl	n.d.	<bdl	<bdl	<bdl	<bdl	n.d.	<bdl	0.001	<bdl	<bdl	0.04	0.05	<bdl	<bdl
Ba	<bdl	<bdl	<bdl	<bdl	<bdl	0.06	0.06	0.02	0.10	0.02	4.07	1.43	2.28	2.25	1.48
La	<bdl	0.004	<bdl	<bdl	<bdl	0.02	0.04	0.004	<bdl	0.002	108	111	13.0	3.04	3.30
Ce	0.01	0.01	<bdl	0.004	<bdl	0.11	0.37	0.01	0.003	0.003	298	344	45.1	11.2	10.4
Pr	<bdl	0.01	<bdl	<bdl	0.00	0.05	0.15	0.01	<bdl	0.002	53.0	55.5	8.23	2.27	1.78
Nd	0.09	0.25	0.02	0.02	0.01	0.49	1.45	0.05	0.02	0.02	267	300	48.0	12.5	10.6
Sm	0.52	1.72	0.06	0.04	0.01	0.53	1.47	0.04	0.02	0.03	92.5	106	20.1	7.30	4.45
Eu	0.53	1.66	0.10	0.04	0.03	0.29	0.60	0.03	0.02	0.00	38.0	43.5	10.1	4.21	1.97
Gd	4.38	8.85	0.91	0.43	0.22	0.91	1.69	0.12	0.07	0.05	70.5	102	23.4	9.88	6.31
Tb	1.72	1.92	0.70	0.28	0.16	0.14	0.20	0.04	0.02	0.02	5.29	11.8	3.48	1.39	1.27
Dy	14.6	12.6	11.0	2.29	2.58	0.43	0.60	0.26	0.17	0.15	10.9	31.5	12.8	7.95	7.91
Ho	3.67	2.57	4.38	0.58	1.12	0.05	0.06	0.05	0.03	0.03	0.98	2.09	1.01	1.11	1.71
Er	9.59	6.93	15.0	1.98	4.36	0.08	0.09	0.09	0.08	0.03	0.93	1.60	0.90	1.58	3.39
Tm	1.41	1.03	2.39	0.31	0.83	0.01	0.01	0.01	0.003	0.01	0.07	0.09	0.06	0.12	0.40
Yb	8.89	7.13	16.6	2.09	6.68	0.04	0.04	0.05	0.03	0.62	0.31	0.32	0.20	0.39	1.93
Lu	1.26	0.97	2.23	0.37	1.08	0.003	0.004	0.01	0.006	0.005	0.03	0.03	0.01	0.03	0.18
Hf	0.13	0.08	0.03	0.03	0.09	0.55	0.59	0.65	0.25	0.47	0.71	0.08	0.06	0.10	0.10
Ta	0.002	0.001	<bdl	<bdl	<bdl	0.02	<bdl	<bdl	<bdl	<bdl	<bdl	0.01	0.04	<bdl	<bdl
Pb	0.04	0.02	0.01	0.02	<bdl	0.58	1.73	0.15	0.10	0.07	23.1	102	76.6	9.95	1.42
Th	<bdl	<bdl	<bdl	0.001	<bdl	<bdl	<bdl	<bdl	0.01	<bdl	4.20	2.76	0.24	0.10	0.18
U	<bdl	<bdl	<bdl	0.001	<bdl	0.01	<bdl	<bdl	0.002	<bdl	8.03	1.08	5.32	0.18	0.07

(continued on next page)

Table 5 (*continued*)

	Phengite			Apatite			Amphibole			Zircon			Rutile			Kyanite
Sample	P_CM15/01	P_CM27/03	P_CM41/01	P_CM15/01	S_SJ4	P_CM27/03	P_CM41/01	P_CM40/03	S_SKP2	P_CM40/03	P_CM27/03	S_SKP17	P_CM15/01	P_CM40/03	S_SKP2	S_SK30
Lithology	Low-Mg	Low-Mg	High-Mg	Low-Mg	Low-Mg	Low-Mg	High-Mg	Low-Mg	Low-Mg	Low-Mg	Low-Mg	Low-Mg	Low-Mg	Low-Mg	Low-Mg	High-Mg
No. of analyses	(1)	(2)	(1)	(2)	(3)	(1)	(2)	(2)	(1)	(3)	(1)	(3)	(4)	(1)	(1)	(1)
Li	n.d.	16	8.31	n.d.	3	<bdl	0.85	14.7	n.d.	<bdl	<bdl	<bdl	<bdl	<bdl	n.d.	1
Sc	3.5	3.33	4.98	<bdl	0.45	<bdl	16.9	31.5	33	1048	918	144	2.38	1.03	3	2
Ti	4137	3948	3887	<bdl	<bdl	2.88	1190	3499	3177	<bdl	<bdl	0.03				48
V	427	339	337	1.7	3.37	0.85	148	440	444	0.18	0.20	38	1889	1609	1395	56
Cr	357	1241	1533	1.35	0.96	1.60	753	156	220	<bdl	2.08	55	539	622	652	1740
Co	n.d.	7.34	5.12	n.d.	0.58	1.03	0.48	75.4	95	<bdl	<bdl	13	0.15	<bdl	0.4	<bdl
Rb	269	157	98	<bdl	0.08	<bdl	0.89	3.27	4.3	<bdl	<bdl	<bdl	<bdl	<bdl	0.00	<bdl
Sr	192	79.0	67.2	1595	538	405	5.03	63.6	73.4	0.54	0.76	0.07	1.04	0.64	1.8	0.07
Y	0.06	0.004	<bdl	48.0	56.1	39.0	0.84	6.33	8.48	149	88.0	69.9	0.10	0.08	0.34	<bdl
Zr	0.67	0.90	0.49	<bdl	0.19	0.94	3.18	8.34	8.79				292	287	304	<bdl
Nb	0.20	0.24	0.18	<bdl	0.17	0.59	0.01	0.05	0.04	1.63	1.30	1.46	147	126	147	<bdl
Cs	7.73	3.61	2.19	n.d.	0.60	<bdl	<bdl	0.02	0.02	<bdl	<bdl	0.01	<bdl	<bdl	n.d.	<bdl
Ba	823	710	695	0.04	0.55	0.19	1.71	3.96	6.99	<bdl	0.07	0.08	<bdl	<bdl	n.d.	<bdl
La	0.01	0.01	<bdl	1.62	0.72	0.26	<bdl	0.01	0.01	0.01	<bdl	<bdl	<bdl	<bdl	<bdl	<bdl
Ce	<bdl	<bdl	<bdl	9.15	0.94	1.18	0.002	0.04	0.06	0.55	0.28	0.04	0.01	<bdl	<bdl	<bdl
Pr	<bdl	<bdl	<bdl	2.50	0.35	0.35	<bdl	0.02	0.04	0.01	<bdl	<bdl	<bdl	<bdl	<bdl	<bdl
Nd	<bdl	<bdl	<bdl	19.8	2.27	2.13	0.01	0.23	0.49	0.13	0.08	0.12	<bdl	<bdl	0.04	<bdl
Sm	0.01	<bdl	<bdl	16.3	2.26	1.38	0.03	0.46	1.01	0.15	0.09	0.08	<bdl	<bdl	<bdl	0.03
Eu	0.01	0.004	<bdl	6.85	1.11	0.78	0.01	0.20	0.51	0.14	0.07	0.07	0.05	0.03	0.01	0.01
Gd	<bdl	<bdl	<bdl	32.9	6.58	4.34	0.03	1.37	2.28	1.89	0.57	0.60	<bdl	<bdl	0.04	<bdl
Tb	<bdl	<bdl	<bdl	3.72	1.97	1.23	0.01	0.31	0.39	0.77	0.35	0.38	<bdl	<bdl	<bdl	<bdl
Dy	0.01	<bdl	<bdl	14.0	12.4	8.23	0.12	1.40	1.96	9.48	5.04	4.65	<bdl	<bdl	0.03	0.01
Ho	<bdl	<bdl	<bdl	1.66	2.10	1.51	0.04	0.28	0.34	4.74	2.65	2.46	<bdl	0.01	0.02	<bdl
Er	<bdl	<bdl	<bdl	2.55	4.20	2.82	0.12	0.60	0.82	25.9	13.5	10.6	0.02	0.03	0.01	<bdl
Tm	<bdl	<bdl	<bdl	0.23	0.46	0.25	0.01	0.08	0.10	7.08	3.93	2.43	<bdl	0.01	<bdl	<bdl
Yb	0.02	<bdl	<bdl	0.89	2.31	1.09	0.04	0.45	0.54	83.4	45.5	29.6	<bdl	<bdl	0.04	<bdl
Lu	<bdl	<bdl	<bdl	0.11	0.22	0.16	0.01	0.06	0.08	22.3	13.3	7.01	<bdl	0.01	0.00	<bdl
Hf	<bdl	0.03	<bdl	<bdl	0.02	<bdl	0.02	0.58	0.62	10231	7949	12158	12.60	12.44	12.08	<bdl
Ta	0.20	0.04	0.02	0.01	<bdl	0.68	<bdl	<bdl	<bdl	0.19	0.13	0.04	9.04	10.71	8.24	<bdl
Pb	5.09	2.00	1.91	1.03	4.86	4.95	0.56	2.48	6.01	0.12	0.10	0.11	0.08	<bdl	0.01	<bdl
Th	<bdl	0.11	<bdl	0.02	0.02	0.00	<bdl	0.002	<bdl	1.91	2.06	1.03	0.004	<bdl	<bdl	0.00
U	<bdl	<bdl	<bdl	0.40	0.37	0.18	<bdl	<bdl	<bdl	11.2	3.48	1.80	0.10	0.12	0.72	<bdl

to 250 Ma, range from +7.4 to +8.2. Initial $^{87}Sr/^{86}Sr$ ratios range between 0.70292 and 0.70705.

6. Mineral chemistry

6.1. Eclogite protolith minerals

The precursor gabbros have a medium to coarse-grained igneous texture and consist of plagioclase, clinopyroxene ± orthopyroxene ± olivine. Plagioclase compositions range from An_{60} to An_{76} in unaltered domains of different samples. Plagioclase REE patterns are characterized by a steady decrease from La to Yb (La_N/Yb_N=31.5) and a distinct positive Eu anomaly (Eu_N/Eu_N*=20) (Table 4, Fig. 6). Incipient alteration results in cloudy areas with extremely fine-grained kyanite, zoisite ± Ca-rich garnet ± sodic clinopyroxene. Primary igneous clinopyroxene appears dark and cloudy due to the exsolution of very fine-grained ilmenite in addition to exsolution of orthopyroxene (Miller et al., 2005b). Analysed clinopyroxene grains are diopside ($Wo_{46–49}En_{43–46}Fs_{6–10}$) containing 4.1–4.6 wt.% Al_2O_3, 0.2–0.4 wt.% Cr_2O_3 and 0.7–0.9 wt.% Na_2O. They are LREE depleted with an La_N/Yb_N ratio of 0.09 and a small negative Eu anomaly (Eu_N/Eu_N*=0.8). Sc, Ti, V, Co, Cr, Y and Zr are strongly partitioned into clinopyroxene relative to plagioclase, whereas Sr is concentrated in plagioclase (Table 4, Fig. 6). Orthopyroxene is bronzite ($En_{71–76}$) with 2.2–2.9 wt.% Al_2O_3. Olivine composition ranges between Fo_{76} and Fo_{79}. Trace element compositions of both clinopyroxene and plagioclase are similar to that documented in olivine gabbros produced by fractional crystallization of N-MORB (e.g. Cortesogno et al., 2000).

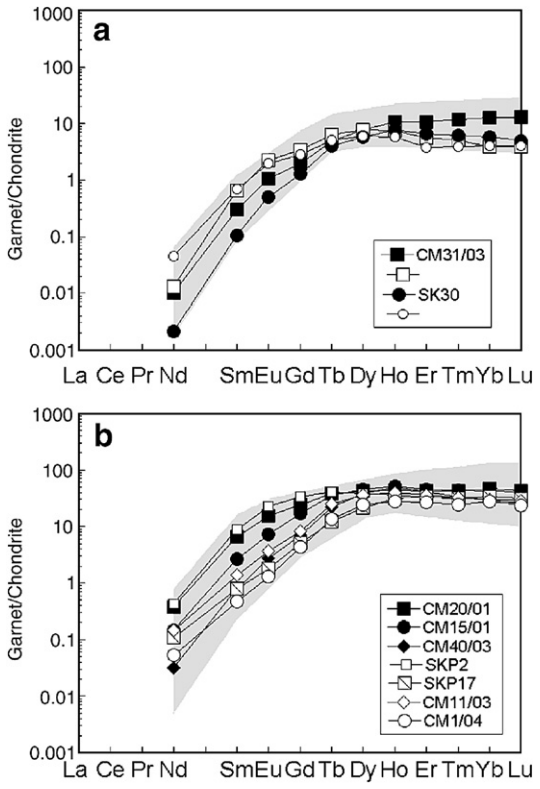

Fig. 7. Chondrite-normalized (Boynton, 1984) REE patterns (shaded areas) in garnet from high-Mg and low-Mg Koralpe, Saualpe and Pohorje eclogites, illustrating (a) core (solid symbols)–rim (open symbols) variations in garnet from high-Mg eclogites CM31/03 and SK30; (b) mean values of garnet in seven different low-Mg eclogites.

6.2. Garnet

Garnet is almandine- and pyrope-rich, with pyrope contents varying from 21 to 59 mol% as a function of both, *P–T* conditions and the bulk-rock mg-number. Garnet with pyrope contents ≥45 mol% is restricted to high-Mg eclogites. In many samples, EPMA profiles and compositional maps of garnet reveal a weak and sometimes irregular major element zoning, usually with increasing X_{Mg} and decreasing X_{Ca} from core to rim. This zoning in major elements suggests garnet growth during prograde metamorphism and that the Mg-rich rims represent peak conditions. Garnet in low-Mg and high-Mg eclogites not only differs with respect to X_{Mg} but also in Ti, V, Cr, Y and REE contents. In high-Mg eclogites, garnet is V- and Cr-rich with moderate Y and very low REE contents, whereas garnet from low-Mg eclogites generally contains less Cr, but higher Y and REE contents (Table 5). Sc (41–88 ppm), Co (50–90 ppm) and Zr (2–10 ppm) concentrations are similar in garnets from both eclogite types (Table 5). Garnet always contains extremely low concentrations of LREE, which made analysis difficult. Chondrite-normalized patterns (Fig. 7) are characterized by a smooth increase in REE from Nd to Tb, and a strong enrichment of HREE over LREE (Yb_N/Ce_N≥1500). As Fig. 7a shows, there is some within-grain variation, with garnet cores always containing higher HREE (and Y) contents compared to rims. In addition to within-grain variations, grain-to-grain HREE, Y, Zr, Cr and Ti variations of up to a factor of 4 were observed, whereas Sc, Co and V usually vary by a factor of ≤2.

6.3. Omphacite

Omphacite is unzoned with respect to major elements and contains 19 to 33 mol% jadeite and ≤2 mol% acmite in high-Mg eclogites. Omphacite in low-Mg

eclogites generally contains 33 to 42 mol% jadeite in addition to 2–5 mol% acmite. Omphacite (Table 5) from low-Mg eclogites is enriched in TiO_2 (0.13–0.18 wt.%), V (463–570 ppm) and depleted in Cr (78–202 ppm) relative to omphacite from high-Mg eclogites (TiO_2 = 0.01–0.03 wt.%; V = 118–303 ppm; Cr = 268–4069 ppm). Omphacite is often the only significant carrier of Li with 13–15 ppm in high-Mg eclogites and 15–131 ppm in low-Mg eclogites. Sr and Pb contents range from 8–70 ppm and from 0.10–2.7 ppm, respectively. Within-grain trace element variations are minor, but grain-to-grain variations within each analysed sample exist although most trace elements vary by a factor of less than 2. Exceptions are Ti and Cr, which may vary by factors of up to 3 and 6, respectively. All analysed omphacites are characterized by bell-shaped

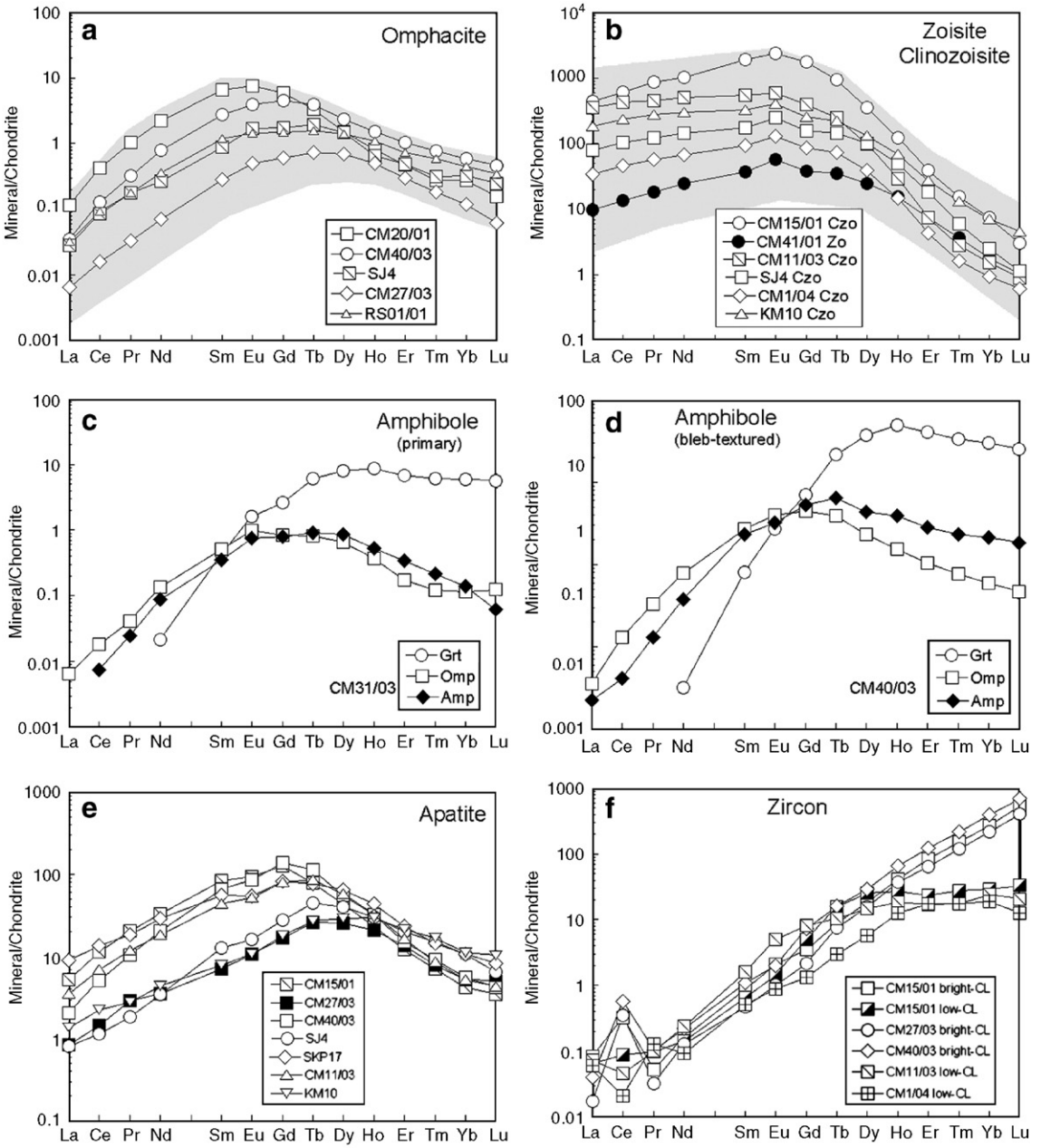

Fig. 8. Chondrite-normalized (Boynton, 1984) REE abundances in (a) omphacite, (b) zoisite/clinozoisite, (c) texturally primary and (d) texturally late amphiboles, together with coexisting garnet and omphacite, (e) apatite, (f) zircon from Koralpe, Saualpe and Pohorje eclogites. Shaded areas represent range of analysed mineral compositions.

chondrite-normalized REE patterns (Fig. 8a), with La_N/Sm_N ranging from 0.02–0.3 and Tb_N/Yb_N ranging from 2.4–24.1. These REE characteristics do not reflect the composition of the primary magmatic clinopyroxene (Fig. 6) and presumably document redistribution of these trace elements among coexisting omphacite, garnet and zoisite/clinozoisite. They are, however, similar to those reported by Messiga et al. (1995) from eclogites derived from Fe–Ti-gabbros from the Ligurian Alps.

6.4. Zoisite/clinozoisite

Fe-poor zoisite with X_{Fe} from 0.022 to 0.025 is common in high-Mg eclogites, whereas clinozoisite (X_{Fe}=0.12–0.16) is restricted to low-Mg eclogites. Allanite was not detected in any of the analysed samples. High-contrast backscattered electron (BSE) images and microprobe analyses revealed the presence of irregular zoning in most grains, particularly in some low-Mg eclogite samples (Fig. 9). Although the zoning seen in BSE images is often due to variable Fe contents, determinations of Ti, Cr, Sr and Ce by EPMA show that within-grain and grain-to-grain variations of Ce and Sr may be large, up to a factor of 10. EPMA analyses compare well with LA-ICP-MS analyses and document that trace element contents of epidote-group minerals vary within and between samples. Zoisite and clinozoisite contain higher concentrations of Sr, Pb and ∑REE (29–3695 ppm), particularly LREE and MREE, than any other co-existing eclogite mineral (Table 5). As suggested by Spandler et al. (2003), the large variations probably reflect the timing of zoisite growth with respect to breakdown of other trace element-rich minerals and/or variations in whole-rock trace element contents. In general, REE, Y, Sr and Pb contents of epidote-group minerals are distinctly lower in the high-Mg cumulate-type eclogites than in the low-Mg eclogites. Analysed zoisite contains 218–1108 ppm Cr, 356–1718 ppm Sr, 138–223 ppm V, 21–45 ppm Y and 1.4–62 ppm Pb. Clinozoisite contains 62–386 ppm Cr, but is generally richer in Sr (1100–4578 ppm), V (213–621 ppm), Y (56–275 ppm) and Pb (8–102) compared with zoisite. Chondrite-normalized REE distribution patterns are depleted in HREE with Ce_N/Yb_N ranging from 1.4–21 in high-Mg eclogites and from 15–189 low-Mg eclogites (Fig. 8b). The positive Eu anomalies (Eu_N/Eu_N*=1.13–1.61) observed in most zoisite and clinozoisite could be related to the breakdown of primary plagioclase (Spandler et al., 2003).

6.5. Amphibole

Calcic amphibole is a minor phase in most samples where it occurs in a number of textural and compositional

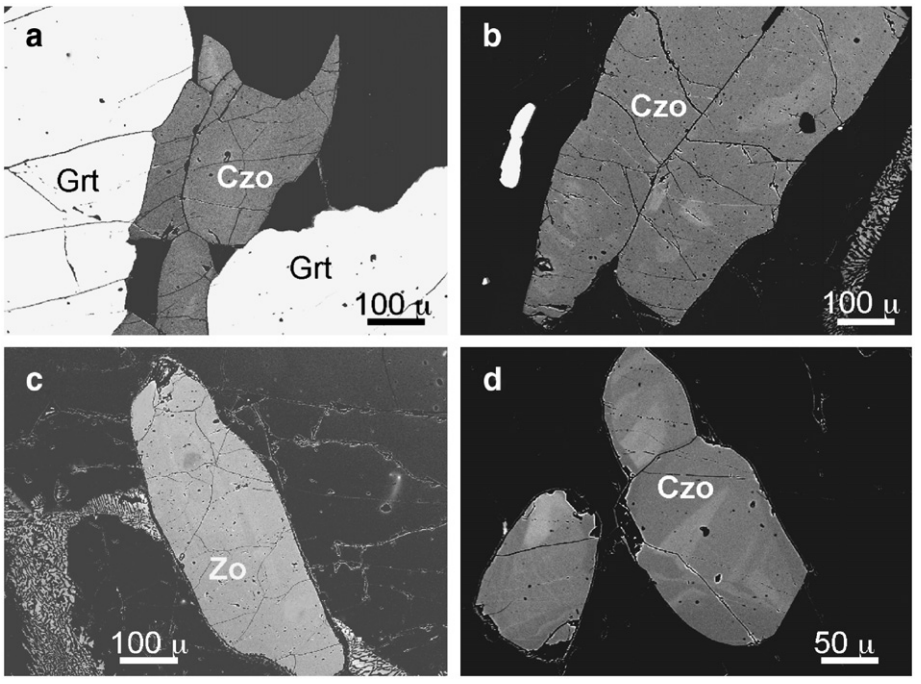

Fig. 9. High-contrast backscattered SEM images to illustrate zoning of zoisite and clinozoisite in Koralpe, Saualpe and Pohorje eclogites. (a) sample CM15/01; (b) sample CM11/03; (c) sample CM41/01; (d) sample CM1/04.

varieties, such as (1) inclusions in garnet and zircon, (2) a matrix phase in textural equilibrium with omphacite and garnet (Fig. 3c), (3) texturally late bleb-textured poikiloblastic grains (Fig. 3d), (4) strongly coloured grains at garnet/omphacite contacts and (5) vermicular intergrowths in symplectite replacing omphacite. Following the classification of Leake et al. (1997), the primary amphiboles are magnesio-hornblendes. They contain less tetrahedral Al and have lower A-site alkalies than the poikiloblastic grains. These bleb-textured amphiboles are edenitic, pargasitic or magnesio-hornblendes with less T-site alumina than other secondary amphiboles. This is compatible with their early formation still at high pressures. Secondary amphiboles in contact with garnet are highly aluminous subsilicic–alumino–pargasite, ferrian–alumino–pargasite, sodian pargasite and pargasitic hornblende. Where amphibole is present in symplectites after omphacite, it is magnesio-hornblende or actinolitic hornblende with distinctly lower Al^{VI} than all other amphiboles.

Most analysed amphiboles are texturally late poikiloblasts with Sr, Rb and Ba contents ranging between 14–75 ppm, 3–10 ppm and 4–16 ppm, respectively. Texturally primary amphibole analysed in high-Mg eclogites CM41/01 and CM31/03 has distinctly lower Sr, Rb, Ba and REE contents. In addition, amphiboles contain 0.5–14 ppm Li, 7–42 ppm Sc, 104–663 ppm V, 123–1421 ppm Cr, 61–92 ppm Co and 4–9 ppm Zr (Table 5). Chondrite-normalized REE patterns are depleted in LREE with Ce_N/Yb_N ratios ranging from 0.004 to 0.06 and Yb_N values of 0.6–4.4. REE patterns of texturally primary amphiboles are similar to those of coexisting omphacite (Fig. 8c), whereas REE patterns of bleb-textured amphibole poikiloblasts always plot between coexisting omphacite and garnet (Fig. 8d), suggesting that these phases are involved in controlling the composition of the texturally late amphiboles.

6.6. Phengite

Phengite with 3.27–3.36 Si apfu is a minor phase and may be present in the matrix or, sporadically, as inclusion in garnet and omphacite. Matrix phengite is always partially replaced by a symplectite consisting of biotite and plagioclase. A slight major element zoning may be present with higher Si and Mg contents in the phengite cores. As only five LA-ICP-MS analyses of four phengite grains from four different eclogite samples are available, no statements about within-grain and grain-to-grain trace element zoning can be made. Phengite is the only eclogite mineral with high Ba (353–823 ppm), Rb (98–269 ppm) and Cs (2.2–7.7 ppm) contents. Phengite also contains appreciable amounts of Sr (78–192 ppm), Cr (172–1533 ppm), Ti (3887–5294 ppm), V (337–505 ppm), Pb (1.9–5.1 ppm) and up to 16 ppm Li. Abundances of other trace elements are very low or below detection limits (Table 5).

6.7. Kyanite

Most analysed kyanite crystals are homogeneous with Cr_2O_3 contents of 0.03–0.57 wt.% and 0.18–0.39 wt.% Fe_2O_3 as main impurities. However, in some high-Mg eclogites, kyanite is zoned with narrow domains that contain up to 1.58 wt.% Cr_2O_3. Except for Cr and V, trace element contents are mostly below detection limits (Table 5).

6.8. Rutile

Rutile crystals are rounded or euhedral and very rarely (<1%) contain inclusions of zircon, omphacite, garnet or apatite. In one sample, an intergrowth between rutile and kyanite was observed. LA-ICP-MS analyses show that rutile contains high concentrations of Cr (229–2566 ppm), V (1031–2245 ppm), Zr (223–360 ppm), Nb (97–258 ppm), Hf (10–17 ppm) and Ta (7–16 ppm). Abundances of Li, Sc, Rb, Sr, Ba, Cs, Y and REE are frequently below detection limits (Table 5), indicating that these elements do not readily enter the rutile structure. Rutile in all analysed eclogite samples has Nb/Ta ratios ranging from 11.8–18.8 with an average of 16.4. This is similar to data for rutile compositions from Trescolmen eclogites (Zack et al., 2002b) and to Nb/Ta ratios of their likely protoliths since MORB and near-axis seamount lavas have Nb/Ta ratios of 12 to 18 (e.g. Niu and Batiza, 1997; Workman and Hart, 2005). It suggests that Nb/Ta ratios remain essentially unchanged during subduction-related dehydration processes as already pointed out by Zack et al. (2002b) and Schmidt et al. (2004).

Because only a few rutile grains were analysed by LA-ICP-MS, an EPMA study allowed data acquisition from a large number of texturally distinct rutile grains from eighteen different Koralpe, Saualpe and Pohorje eclogite localities (Table 6). Within each sample, individual rutile grains are homogeneous, but small grain-to-grain Al and Nb variations and more pronounced variations of Fe and Cr concentrations exist. Fe abundances are generally higher in rutile included in garnet (4045±1415 ppm) compared to matrix rutile (2038±721 ppm) and rutile included in omphacite, zoisite or kyanite (2353±1358 ppm), whereas variations of Cr content of different grains within each sample are

Table 6
Summary of Cr and Zr in rutile measurements and temperatures based on Zr in rutile and garnet–clinopyroxene

Sample	Lithology	Cr (ppm) Average	SD (ppm)	Zr (ppm) Average	SD (ppm)	No. of grains/ spots analysed	Method	*T*(°C)* Zack et al. (2004)	*T*(°C) Watson et al. (2006)	*T*1(°C)** Powell (1985)	*T*2(°C)** Krogh Ravna (2000)
CM15/01	Low-Mg	539	175	292	28	3/4	LA-ICP-MS	715	640	703	644
CM15/01	Low-Mg	528	106	282	7	12/42	EPMA	711	631	703	644
CM17/01	Low-Mg	633	195	288	8	4/4	EPMA	714	639	702	642
CM20/01	Low-Mg	n.d.		252		1/1	LA-ICP-MS	697	628	722	658
CM20/01	Low-Mg	720	174	282	15	8/17	EPMA	711	631	722	658
CM25/01	High-Mg	4801	196	289	7	4/14	EPMA	714	639	747	636
CM41/01	High-Mg	2725	1095	288	10	11/29	EPMA	714	639	741	648
RS01/01	High-Mg	4469	1486	291	19	4/9	EPMA	715	640	746	653
CM20/03	High-Mg	2880	323	281	14	9/33	EPMA	711	637	721	627
CM24/03	High-Mg	2446	890	291	9	6/12	EPMA	715	640	712	635
CM27/03	Low-Mg	2566		334		1/1	LA-ICP-MS	733	651	721	637
CM27/03	Low-Mg	2508	1004	287	24	10/34	EPMA	713	639	721	637
CM28/03	Low-Mg	728	22	295	6	4/8	EPMA	717	641	699	637
CM31/03	High-Mg	3883	1058	288	5	6/13	EPMA	714	639	758	665
CM35/03	High-Mg	5758	508	302	16	7/26	EPMA	720	643	735	607
CM40/03	Low-Mg	621		287		1/1	LA-ICP-MS	713	639	699	651
CM40/03	Low-Mg	794	218	286	9	11/20	EPMA	713	630	699	651
CM1/04	Low-Mg	945	137	287	12	6/26	EPMA	713	639	708	660
H42	Low-Mg	506	109	281	22	7/19	EPMA	711	637	704	657
KM4	Low-Mg	280	90	290	15	6/37	EPMA	715	640	720	635
KM10	Low-Mg	280	135	287	8	11/39	EPMA	713	639	700	661
KK1	Low-Mg	649	162	281	12	12/28	EPMA	711	637	688	639
SKP2	Low-Mg	652		304		1/1	LA-ICP-MS	721	644	711	655
SKP2	Low-Mg	464	72	313	18	12/45	EPMA	724	646	711	655
88T35	High-Mg	2781	1238	312	23	10/33	EPMA	724	646	731	654
40T30	High-Mg	987	1015	305	15	6/25	EPMA	721	644	730	648
SKP12	High-Mg	4224	995	317	11	15/48	EPMA	726	647	717	647
SKP17	Low-Mg	881	380	311	14	12/25	EPMA	724	645	713	648
SKP23	High-Mg	1150	707	319	18	22/62	EPMA	727	647	717	639
SKP27	High-Mg	1699	512	298	8	8/28	EPMA	718	642	719	639
SKP28	Low-Mg	771	118	300	11	2/7	EPMA	719	642	720	643
CM11/03	Low-Mg	782	108	320	19	8/27	EPMA	727	648	698	629
SK12	High-Mg	5623	1018	304	14	11/31	EPMA	721	644	733	642
SJ4	Low-Mg	708		313		1/1	LA-ICP-MS	724	646	688	626
SJ4	Low-Mg	670	135	306	16	12/55	EPMA	721	644	688	626
89T63	Low-Mg	595	48	309	16	6/15	EPMA	723	645	698	647
89T66	Low-Mg	239	41	292	10	8/17	EPMA	715	640	696	655

*Calculated with Eq. (4) of Zack et al. (2004); **calculated for a nominal pressure of 2.4 GPa.
P = Pohorje; K = Koralpe; S = Saualpe.

independent of the microtextural site. Average Cr abundances of rutile from different samples however, show large variations and vary from 239 ppm to 5623 ppm. Average Cr concentrations of rutile are positively correlated with the whole-rock Cr content, with rutile from cumulate-derived high-Mg eclogites being distinctly richer in Cr than rutile from low-Mg samples (Fig. 10a). For different samples, average Nb and Al contents range from 36 to 240 ppm and from 38 to 495 ppm, respectively. Measured Zr concentrations, however, are remarkably similar and do not correlate with either whole-rock Cr contents (Fig. 10b) nor with Cr and Fe concentrations in rutile (Fig. 10c, d). Rutile inclusions in garnet (214 analyses of 101 individual grains from 29 samples) contain an average of 296± 14 ppm Zr, rutile inclusions in omphacite, kyanite or

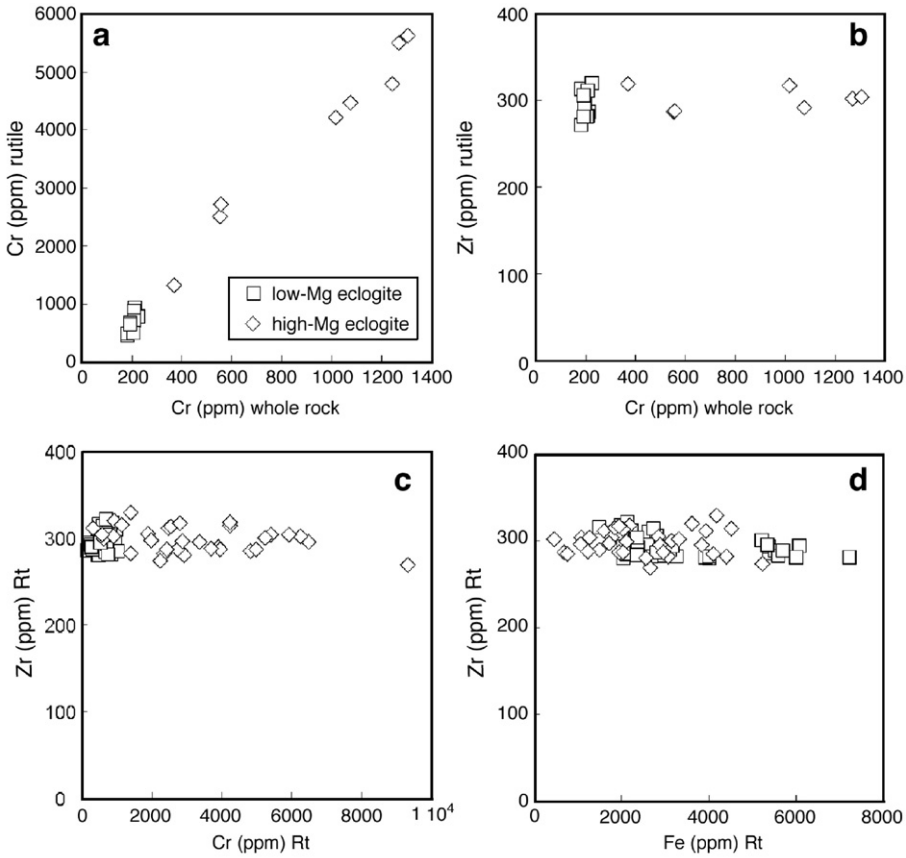

Fig. 10. (a) Plot of average Cr in rutile vs. Cr contents in corresponding whole rocks showing that variations in whole-rock Cr concentrations are reflected in the Cr contents of rutile. High-Mg eclogites are characterized by Cr contents > 500 ppm. (b) Plot of average Zr in rutile vs. Cr contents in whole rocks. Variation diagrams of (c) Cr and Zr and (d) Fe and Zr concentrations in rutile (matrix rutile and rutile included in garnet, omphacite, zoisite and kyanite) from different Koralpe, Saualpe and Pohorje eclogite localities illustrating that Zr in rutile is buffered by the presence of zircon.

zoisite (88 analyses of 29 individual grains from 15 samples) average 293 ± 13 ppm Zr and matrix rutile (520 analyses of 141 individual grains from 30 samples) contains an average of 297 ± 13 ppm Zr.

6.9. Apatite

Apatite crystals from both eclogite types are commonly rounded and may contain needle-like micro-exsolutions of Fe ± Cu ± Ni sulfides in addition to rare inclusions of rutile. When analysed by EPMA, apatite does not contain any Si and Na, and divalent cations Fe + Mn + Mg that occupy the apatite Ca site range between 0.07 and 0.19 wt.%. Sr contents are variable, ranging from 111–2030 ppm for 38 grains from 12 different eclogite samples, independent of bulk rock Sr concentrations. EPMA analyses also showed that individual apatite grains are homogeneous with respect to Sr, F and Cl, but Sr, F and Cl contents may vary from grain to grain within a given sample. To date, Cl and F contents have been found to range from 0.13–1.73 wt.% and 0.27–2.44 wt.%, respectively, implying calculated H_2O contents ranging from 0. 58 to 1.12 wt.%. This suggests that apatite formed in the presence of saline brines.

LA-ICP-MS analyses confirmed that apatite hosts significant amounts of Sr (405–1686 ppm) and REE (26–165 ppm). Other trace elements present in appreciable amounts are Y (35–80 ppm) and Pb (0.6–19 ppm), but there is considerable compositional variation between samples (Table 5). Chondrite-normalized REE distribution patterns are bell-shaped with a marked relative enrichment of the MREE (Fig. 8e) and La_N/Sm_N and Tb_N/Yb_N ratios of 0.04–0.19 and 4–18, respectively.

6.10. Zircon

Zircon is present as inclusion in garnet (dominant), omphacite, zoisite, kyanite, amphibole, rutile and in the

matrix. Grain size is highly variable, with longest dimensions ranging from approximately 5 to 280 μm. In thin section, zircon crystals are frequently ovoid or rounded. Out of 509 zircon grains studied in thin section so far from Koralpe, Saualpe and Pohorje eclogites, 53 contain mineral inclusions. In order of abundance, these are rutile, omphacite, garnet, apatite, magnesio-hornblende, quartz and kyanite (Fig. 11), clearly indicating a metamorphic origin. Cathodoluminescence (CL) images reveal the absence of distinct zoning, but the presence of bright-CL core domains in most grains (Fig. 11).

Zircon core and rim domains analysed by LA-ICP-MS have very low Pb (<1 ppm), Th (0.01–1.9 ppm) and U (0.24–14.3 ppm) contents and low Th/U ratios ranging from 0.01 to 0.17 (Table 5). Zircon contains 0.79–1.5% Hf, 33–192 ppm Y and 151–1048 ppm Sc, with low-CL domains being richer in Hf, but containing less Y than bright-CL domains. EPM analyses of zircon yielded similar results for Hf (0.83–1.4%) and Y (<62–548 ppm) in addition to P in the range of 159–425 ppm. U and Th contents of zircon core and rim domains were always below detection limits of 39 and 41 ppm, respectively. REE concentrations are variable, with totals between 11 and 200 ppm. Chondrite-normalized REE patterns are enriched in HREE (Yb_N/Nd_N=99–3362) without negative Eu anomalies (Fig. 8f). The patterns show that the analysed bright-CL zircon cores are characterized by a more pronounced fractionation in HREE (Yb_N/Dy_N=16.7–33.3) relative to low-CL domains (Yb_N/Dy_N=1.1–1.7). This suggests contemporaneous growth of zircon rims and garnet since subsolidus formation of garnet depletes the HREE in the reactive bulk, resulting in the HREE patterns of co-crystallizing zircon being nearly flat or with a negative slope (Rubatto, 2002; Whitehouse and Platt, 2003). Moreover, the low Th/U ratios, low Th, U and Y concentrations and the absence of negative Eu anomalies in all analysed zircon core and rim domains indicate a metamorphic origin and zircon formation in the absence of plagioclase (Rubatto, 2002; Hoskin and Schaltegger, 2003).

7. Discussion

7.1. Constraints on the mantle source and on fluid–rock interaction

Both metagabbros and eclogites have NMORB-like Sm–Nd isotope compositions (Table 3), are LREE-depleted and lie in the oceanic gabbro field in incompatible trace element diagrams (Figs. 5, 12a), suggesting that their precursors were derived from a depleted spinel peridotite mantle source. Depleted mantle source characteristics can also be inferred from Fig. 12b as Nb/Zr ratios are not readily affected by variations in the degree of partial melting and fractional crystallization processes and should reflect the primary mantle source. The

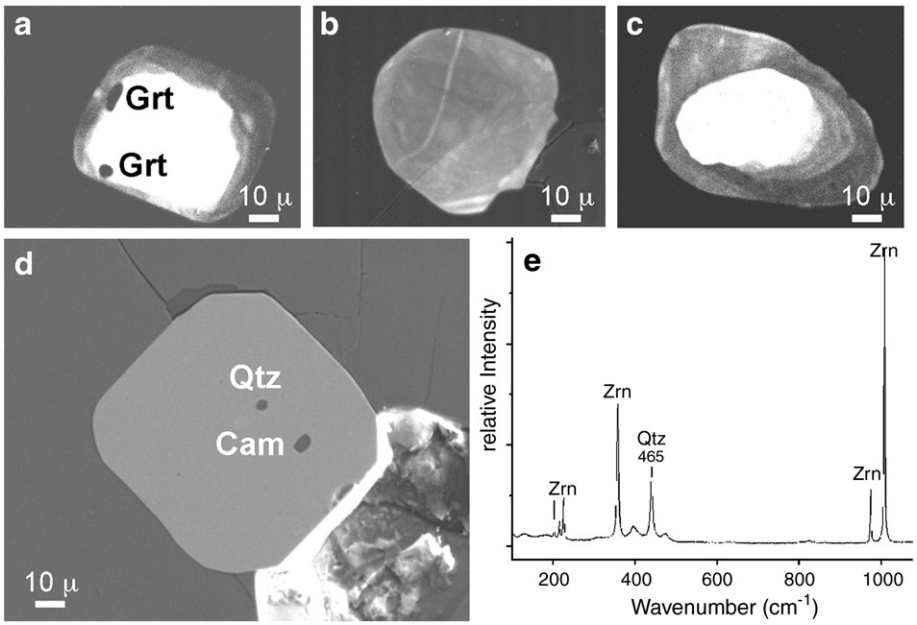

Fig. 11. Zircon in Koralpe, Saualpe and Pohorje eclogites: CL images of (a) zircon containing two inclusions of garnet (89T66); (b) matrix zircon (CM15/01); (c) zircon included in omphacite (H42); (d) SE image of zircon included in zoisite with inclusions of quartz and calcic amphibole (SKP28); (h) Raman spectrum of quartz inclusion in zircon (SKP28).

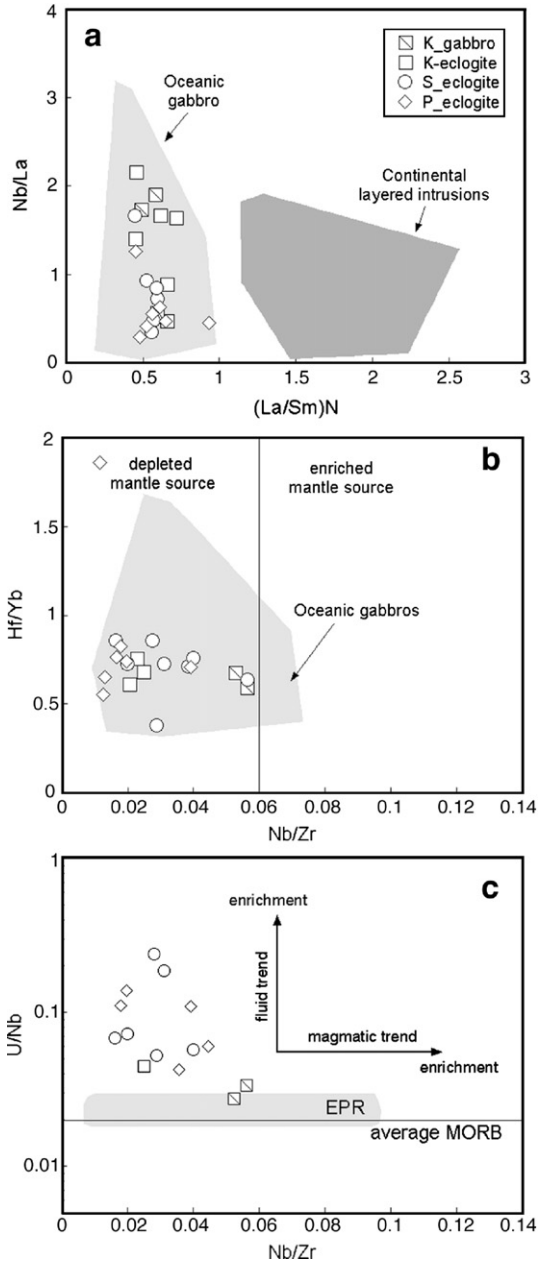

Fig. 12. Plots of (a) Nb/La vs. $(La/Sm)_N$ and (b) Hf/Yb vs, Nb/Zr after John et al. (2004) showing that Koralpe, Saualpe and Pohorje eclogites resemble oceanic gabbros generated in a mid-oceanic environment. (c) Plot of U/Nb vs. Nb/Zr after John et al. (2004) showing that only gabbros have U/Nb ratios similar to those of oceanic basalts, whereas all eclogites have different ratios. Data sources for oceanic gabbros: Ross and Elthon (1997), Constantin (1999), Foulger et al. (2005), http://%2520www-odp.tamu-edu/; for continental gabbros: Cottin et al. (1998), Aït-Djafer et al. (2003), Zhou et al. (2005).

positive Eu-anomalies observed in gabbros and some high-Mg eclogites are due to plagioclase accumulation and similar to anomalies seen in cumulate gabbros typical of the lower oceanic crust (Fig. 5a, b). The REE characteristics of the low-Mg eclogites on the other hand are similar to isotropic gabbros from oceanic crust. The LREE contents of sample CM27/03 ($La_N/Yb_N=1.44$) are decoupled from those of the HREE and HFSE, the concentrations of which are similar to those of the other eclogites (Fig. 5e, f). Its initial Nd isotope composition (Table 3), Nb/Zr and Hf/Yb ratios are within the range observed in the other samples, suggesting that the precursor rock has not crystallized from a partial melt derived from an enriched mantle source.

Eclogitic veins with the same mineralogy as the host rocks and the stability of zoisite/clinozoisite, magnesiohornblende and phengite document the presence of fluids at the time of eclogitisation. The source and timing of fluid influx remain enigmatic, but such fluids could originate by dehydration of the country rocks during subduction (e.g. Wayte et al., 1989) or, more likely, be derived from seawater-altered oceanic crust and/or mantle (e.g. Barnicoat and Cartwright, 1997; Scambelluri et al., 1997; John and Schenk, 2003). The initial $^{87}Sr/^{86}Sr$ ratios of the gabbros and eclogites range between 0.70249 and 0.70705. When viewed on a $\varepsilon(t)$Nd vs. $^{87}Sr/^{86}Sr$ isotope variation diagram (Fig. 13), the gabbros and some high-Mg eclogites plot within the MORB field, whereas the displacement of most eclogite isotope data suggests reaction with evolved seawater or alteration by a fluid maintaining seawater composition. The negative Ce anomaly ($Ce/Ce^*=0.43$) observed in high-Mg eclogite RS01/01 (Fig. 5c) also indicates

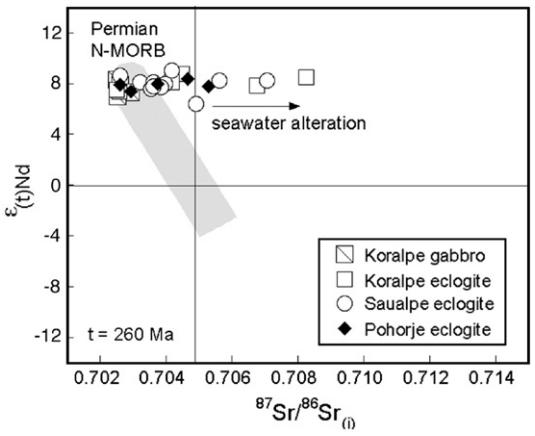

Fig. 13. Nd vs. Sr isotope correlation diagram of Koralpe, Saualpe and Pohorje gabbros and eclogites (including data from Thöni and Jagoutz, 1992; Miller and Thöni, 1997; Miller et al., 2005a). The gabbroic protoliths and most of the kyanite-rich eclogites plot on the Mantle array. The Sr isotopic composition of eclogites that plot to the right of the Mantle array could have been altered by reactions with seawater (e.g. Muehlenbachs, 1986).

seawater alteration. The gabbros retained U/Nb ratios similar to MORB (i.e., 0.2; Hofmann et al., 1986), but the eclogites plot outside the ocean basalt range (Fig. 12c), suggesting secondary addition of highly soluble U from seawater (Kelley et al., 2005). The presence of Cl-amphibole in partially reacted metagabbros and Cl-apatite in eclogites suggests recycling of seawater-derived chlorine-rich fluids. All samples, however, have Ce/Pb ratios (0.2–10.4) distinctly lower than MORB (i.e., 25±5; Hofmann et al., 1986), indicating addition of Pb by a different fluid. As argued by John et al. (2004), infiltration of gabbros and eclogites by a Pb-rich fluid could have occurred during exhumation or during continental collision.

7.2. Whole-rock elemental budgets and retention of trace elements

For the analysed gabbro, mass balance calculations indicate that plagioclase dominates the Rb and Sr budget of the whole rock and clinopyroxene dominates MREE, HREE, Y, Ti, Sc and V (Fig. 14a). Calculated values for La, Ce, Pb, U, Th, Zr, Hf and Nb are much less than whole-rock compositions. These deficits could possibly be accounted for by the presence of non-analysed apatite, ilmenite and zircon.

The distribution of trace elements among the minerals of a low-Mg and a high-Mg eclogite was calculated using mineral modes determined by thin-section observation and average trace-element mineral compositions. Samples CM15/01 and CM41/01 were selected on the basis of textural equilibrium and relatively homogeneous mineral compositions. Although average trace element compositions of garnet, zoisite and clinozoisite are not accurate because of zoning, the calculated trace-element budgets (Fig. 14b, c) show that the distribution of many trace elements is quite well constrained. For Li and Cs, no whole-rock data exist and the calculated whole-rock values were normalized to 100%. Li contents of the eclogites, estimated by multiplying mineral Li concentrations with their modal fractions, range from 3 to 59 ppm. This is similar to the Li range found in fresh (Chan et al., 1992) and low-T altered MORB (Tomascak et al., 2002), in the Trescolmen eclogites, interpreted to have derived from basaltic protoliths with variable degrees of low-T seafloor alteration (Zack et al., 2003) and in eclogites from collisional belts (Woodland et al., 2002).

The Sr analyses of major and accessory minerals demonstrate that epidote-group minerals, phengite, omphacite and apatite are the major Sr-bearing phases under high-pressure conditions where calcic plagioclase

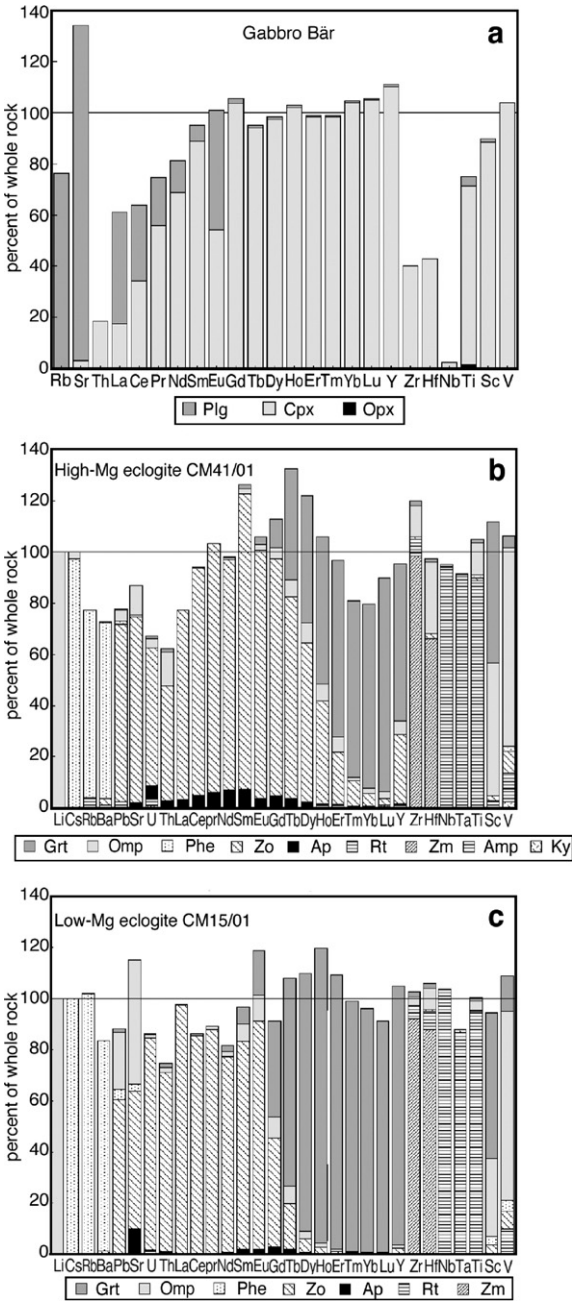

Fig. 14. Trace element budgets for (a) a gabbroic eclogite protolith, (b) high-Mg eclogite CM41/01 and (c) low-Mg eclogite CM15/01. The distribution of trace elements among the minerals was calculated using average mineral trace-element compositions and relative proportions of the minerals. See text for explanation.

is unstable. Clinozoisite and zoisite are always richer in Sr than coexisting apatite, phengite and omphacite. Zoisite/clinozoisite is also a major carrier of LREE, Th, U and Pb in the investigated eclogites. These results compare well with the studies of Hermann (2002), Zack

et al. (2002a) and Spandler et al. (2003) documenting that epidote-group minerals may host up to 95% of U, Th, Pb, Sr and LREE in high-grade mafic rocks. Zoisite or allanite that may form at the expense of zoisite at high pressure (Hermann, 2002) are common constituents of eclogites derived from oceanic crust (e.g. Schmidt and Poli, 1998; Zack et al., 2002a). The presence or absence of these phases should control recycling of these elements in subduction zone environments (e.g. Tribuzio et al., 1996; Nagasaki and Enami, 1998; Hermann, 2002; Spandler et al., 2003).

Omphacite can host significant quantities of Sr, Pb, Li and V. Garnet contains most of the HREE, Y, and significant proportions of Sc. Rutile accounts for most of the Nb, Ta and Ti, whereas zircon hosts most of the Hf and Zr. Phengite contains nearly all Cs, Rb and Ba, plotting in the field of low-T altered MORB in the Cs/Rb versus Ba/Rb diagram (Fig. 15). As phengites contain most of the whole-rock budget for these elements and mirror the Cs/Rb and Ba/Rb ratios of their host rocks (Zack et al., 2001) this suggests low-T ocean-floor alteration prior to subduction in accordance with whole-rock Ba/Rb ratios of 5.9–9.3 and elevated $^{87}Sr/^{87}Sr$ ratios of 0.70464–0.70528 of phengite-bearing eclogite samples.

As this study of the Koralpe, Saualpe and Pohorje eclogites does not reveal any significant changes in major and trace element compositions during the gabbro-to-eclogite transformation, the mafic material did not experience extensive loss of fluid-mobile elements due to breakdown of hydrous minerals. This confirms previous studies that demonstrated that mineral stabilities control the trace element systematics of mafic systems in subducting crust (Tribuzio et al., 1996; Hermann, 2002; Zack et al., 2002a; Spandler et al., 2003, 2004). Although

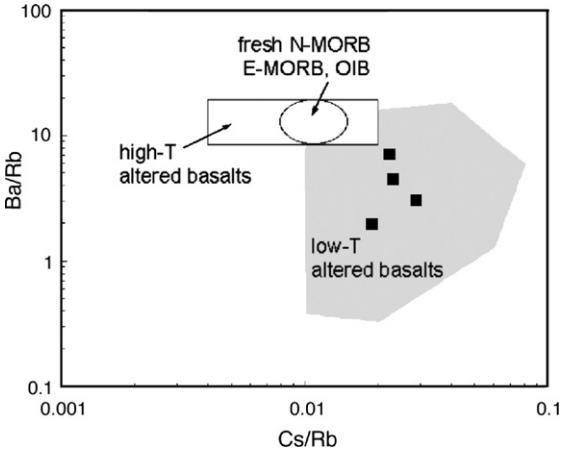

Fig. 15. Ba/Rb vs. Cs/Rb plot after Zack et al. (2001), illustrating phengite compositions and likely protoliths.

breakdown of hydrous phases releases significant amounts of water over a wide range of P and T conditions, most trace elements are redistributed into newly formed minerals. Hence, dehydration processes and trace element release are largely decoupled, allowing preservation of magmatic trace element whole-rock characteristics even at ultrahigh pressure conditions.

Since allanite and phengite host most of LILE, LREE and Th, only the disappearance of these minerals by dissolution in hydrous granitic melts (Hermann, 2002) or by melting in the presence of fluids (Hermann and Green, 2001) could induce transfer of these elements from subducting crust and thereby change the geochemical signature of eclogites inherited from their mafic precursor rocks.

7.3. Trace element partitioning and rutile thermometry

Knowledge of partition coefficients (*D*-values) of trace elements among coexisting minerals is useful for establishing trace element equilibrium. Although many minerals are in textural equilibrium, trace element zoning prevents any precise evaluation of *D*-values. The partitioning of trace elements between different eclogite minerals was calculated using average trace element concentrations and is summarised in Fig. 16, showing that patterns of relative distribution are similar for all analysed Koralpe, Saualpe and Pohorje eclogites. The wide spread in absolute *D*-values is not only a consequence of the extremely low contents (<100 ppb) of Ba, Th, Nb, Ta, U and LREE in analysed garnet and clinopyroxene but also reflects inhomogeneous trace element distributions in the sample suite. Even so, the *D*-values are within the range reported for eclogites from the Ligurian Alps (Messiga et al., 1995), the Adula nappe (Bocchio et al., 2000; Zack et al., 2002a), for coesite-bearing eclogites from Dabieshan (Sassi et al., 2000) and for high-temperature mantle eclogites (Harte and Kirkley, 1997), suggesting that there is no strong pressure and temperature dependence (Fig. 17). The large spread of partition coefficients between omphacite and garnet seen in Fig. 17, however, also indicates that these data sets include elemental concentrations that reflect trace element disequilibrium between minerals in eclogite-facies rocks. This agrees with other studies that demonstrated incomplete trace element equilibrium in eclogites (Thöni and Jagoutz, 1992; Messiga et al., 1995; Zack et al., 2002a; Spandler et al., 2003).

Although most analysed minerals are not homogeneous with respect to trace elements, an approach to local equilibrium is suggested by the good correlation of Sm concentrations where measured near rims of coexisting garnet and omphacite. Over a concentration range of two

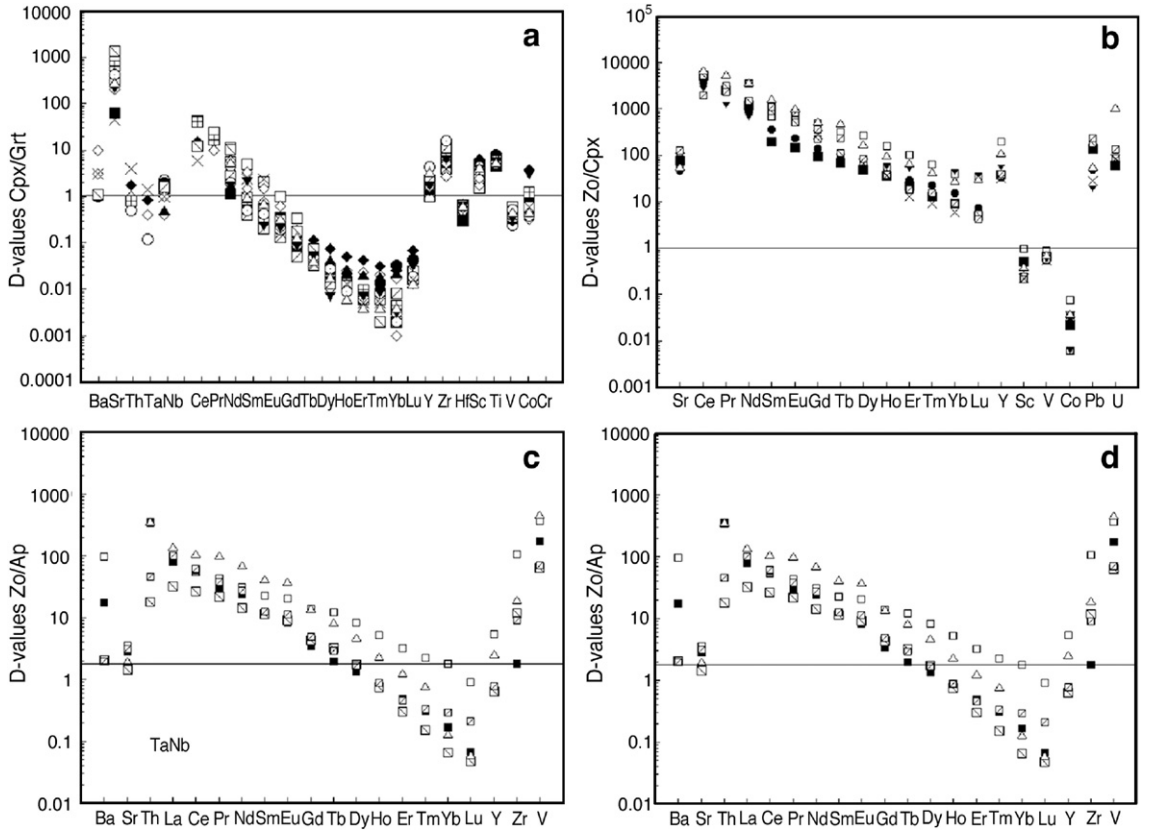

Fig. 16. Partition coefficients of (a) omphacite/garnet, (b) zoisite/omphacite in kyanite-(solid symbols) and quartz-rich (open symbols) Koralpe, Saualpe and Pohorje eclogites, calculated using average trace element compositions. *D*-values for La are not included due to analytical uncertainties caused by the extremely low concentrations of La in garnet and omphacite. See text for discussion.

orders of magnitude samples lie on a straight line passing through the origin, demonstrating similar clinopyroxene–garnet partition coefficients. In addition, small-scale equilibrium is indicated by rather constant Zr contents of rutile coexisting with zircon (Table 6).

Zack et al. (2002b) demonstrated a temperature dependence of Zr in rutile in zircon-buffered mineral assemblages. More recently, Zack et al. (2004) published an empirical rutile thermometer applicable to rutile+zircon+quartz assemblages and Watson et al. (2006) presented a Zr in rutile geothermometer based on combined experimental and natural results. As most of the investigated Koralpe, Saualpe and Pohorje eclogites contain the required buffering assemblage (Fig. 18), Zr concentrations were determined by EPMA in a large number of rutile grains (822 analyses of 271 individual grains) in order to assess homogeneity within and between grains. The results show that rutile is unzoned and Zr concentrations are not correlated with textural setting since compositions of rutile inclusions within garnet, omphacite, zoisite or kyanite are similar to those

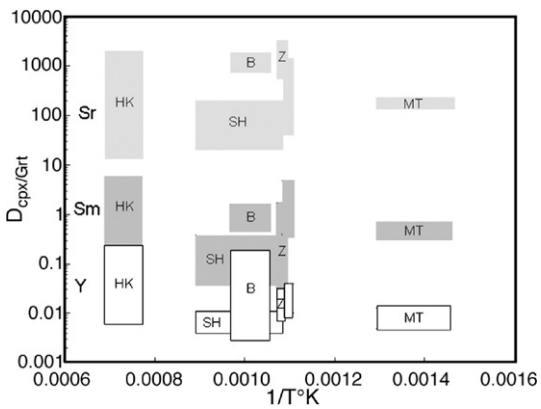

Fig. 17. Plot of Sr (light grey), Sm (dark grey) and Y (white) partitioning between omphacite and garnet in different eclogites vs. Temperature. HK = Roberts Victor mantle eclogites, estimated $P=3$–5 GPa (Harte and Kirkley, 1997); SH = Dabie Shan, estimated $P=3$ GPa (Sassi et al., 2000); B = Soazza, estimated $P\geq 1.5$ GPa (Bocchio et al., 2000); Z = Trescolmen, estimated $P=2.4$ GPa (Zack et al., 2002a); MT = Gruppo di Voltri, estimated $P=2$ GPa (Messiga et al., 1995); unmarked boxes=this work, estimated $P=2.4$ GPa. See text for discussion.

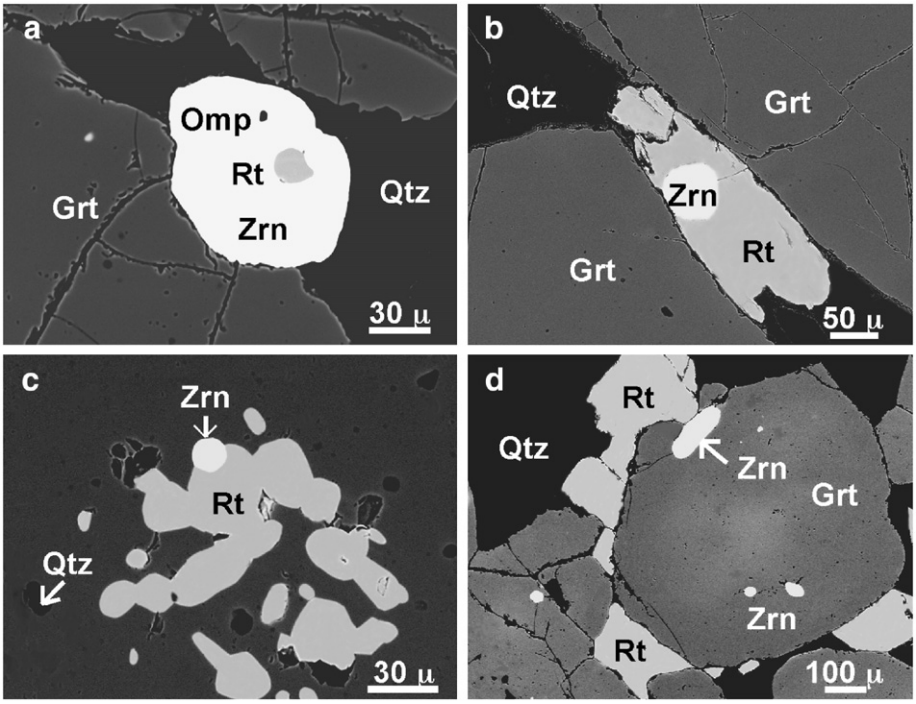

Fig. 18. BSE images showing rutile microtextures in eclogites: (a) zircon with inclusions of rutile and omphacite (sample CM1/04, Koralpe); (b) anhedral matrix rutile containing an inclusion of zircon (sample CM20/01, Pohorje); (c) matrix rutile intergrown with zircon (sample KK1, Koralpe); (d) anhedral matrix rutile next zircon and quartz (sample 89T66, Saualpe).

of matrix rutile. Moreover, the presence of rutile, zircon and quartz inclusions within garnet indicates that these minerals co-crystallized during peak metamorphic conditions dated at 90 Ma (Miller et al., 2005a). Zr variations are limited (Table 6), suggesting an approach to equilibrium of the Zr distribution between rutile and zircon at temperatures of 700–730 °C according to Zack et al. (2004) or in the range of 630–650 °C according to Watson et al. (2006). This discrepancy cannot be solved easily as the results based on the Zr-in-rutile thermometer of Watson et al. (2006) are consistent with temperatures based on the Krogh Ravna (2000) calibration of the temperature-dependent Fe^{2+}–Mg^{2+} partitioning between garnet and omphacite (Table 6), whereas temperatures calculated with Eq. (4) of Zack et al. (2004) are consistent with temperatures based on Powell (1985), Brandelik and Massonne (2004) and Krogh Ravna and Terry (2004). In addition, as discussed by Watson et al. (2006) the effect of pressure on the Zr-in-rutile thermometry is not yet completely understood and might result in a temperature underestimate of about 35 °C from using their nominally 1 GPa thermometer. Rutile included in garnet, omphacite or kyanite and matrix rutile yield similar temperatures suggesting that crystallization of rutile in the matrix does not reflect growth with increasing temperature during metamorphism nor during cooling. No systematic variation in rutile temperatures was observed from N to S, consistent with the Koralpe, Saualpe and Pohorje domain having behaved as a coherent block during subduction.

8. Conclusions

The geochemistry of the Koralpe, Saualpe and Pohorje eclogites shows that they were derived from gabbroic intrusions. Gabbros and eclogites have NMORB-like initial Nd isotope and trace element compositions indicating that their parental melts were derived from a depleted mantle source. The gabbro to eclogite transition did not induce major changes in the whole-rock REE compositions, suggesting REE redistribution into newly formed garnet, omphacite and zoisite/clinozoisite during high-pressure metamorphism. This confirms other recent studies showing that dehydration of oceanic crust alone appears to be insufficient to liberate the necessary LILEs, U and Pb observed in arc lavas. Chemical heterogeneities inherent in the gabbroic precursor rocks are responsible for distinct trace element contents of high-Mg and low-Mg–eclogites. Thus, garnet, omphacite and clinozoisite in low-Mg eclogites are characterized by

distinctly higher REE and other incompatible trace element contents than garnet, omphacite and zoisite in high-Mg eclogites derived from early cumulates. This is important to bear in mind when selecting garnet and omphacite with Sm, Nd, Lu and Hf concentrations suitable for dating.

In quartz- and zircon-bearing eclogites, Zr-in-rutile thermometry recently calibrated by Zack et al. (2004) and Watson et al. (2006) is an attractive method to assess the approach to equilibrium and to calculate high-precision temperatures in eclogites. If these temperatures can be linked to U–Pb zircon dates and/or pressure-sensitive reactions, *P–T–t* points can be established for subduction complexes, thereby improving our knowledge of subduction tectonics.

Acknowledgements

Financial support by the Austrian Science Foundation (FWF), project P13227-GEO, and by the University of Innsbruck is gratefully acknowledged. We thank R. Kaindl of the Christian Doppler Laboratory, University of Innsbruck, for the assistance with laser Raman spectroscopy. We would also like to thank T. Zack (Heidelberg) for providing synthetic rutile with known trace element contents. Constructive reviews by C. Spandler and an anonymous reviewer, and the editorial handling by R. Rudnick helped to improve the paper.

References

Ahrens, T.J., Schubert, G., 1975a. Rapid formation of eclogite in a slightly wet mantle. Earth Planet. Sci. Lett. 27, 90–94.

Ahrens, T.J., Schubert, G., 1975b. Gabbro–eclogite reaction and its geophysical significance. Rev. Geophys. Space Phys. 13, 383–400.

Aït-Djafer, S., Ouzegane, K., Liégois, J.P., Kienast, J.R., 2003. An example of post-collisional magmatism: the layered gabbro–anorthosite complex from Tin Zebane area (western hoggar, Algeria). J. Afr. Earth Sci. 37, 313–330.

Barnicoat, A.C., Cartwright, I., 1997. The gabbro–eclogite transformation: an oxygen isotope and petrographic study of west Alpine ophiolites. J. Metamorph. Geol. 15, 93–104.

Becker, H., Jochum, K.P., Carlson, R.W., 2000. Trace element fractionation during dehydration of eclogites from high-pressure terranes and the implications for element fluxes in subduction zones. Chem. Geol. 163, 65–99.

Bocchio, R., De Capitani, L., Ottolini, L., Cella, F., 2000. Trace element distribution in eclogites and their clinopyroxene garnet pair: a case study from Soazza (Switzerland). Eur. J. Mineral. 12, 147–161.

Boynton, W.V., 1984. Cosmochemistry of the rare earth elements: meteorite studies. In: Henderson, P. (Ed.), Rare Earth Element Geochemistry. Elsevier, Amsterdam, pp. 63–114.

Brandelik, A., Massonne, H.J., 2004. PTGIBBS—an EXCEL™ Visual Basic program for computing and visualizing thermodynamic functions and equilibria of rock-forming minerals. Comput. Geosci. 30, 909–923.

Chan, L.H., Edmond, J.M., Thompson, G., Gillis, K., 1992. Lithium isotopic composition of submarine basalts: implications for the lithium cycle in the oceans. Earth Planet. Sci. Lett. 108, 151–160.

Constantin, M., 1999. Gabbroic intrusions and magmatic metasomatism in harzburgites from the Garret transform fault: implications for the nature of the mantle–crust transition at fast spreading ridges. Contrib. Mineral. Petrol. 136, 111–130.

Cortesogno, L., Gaggero, L., Zanetti, A., 2000. Rare earth and trace elements in igneous and high-temperature metamorphic minerals of oceanic gabbros (MARK area, Mid-Atlantic Ridge). Contrib. Mineral. Petrol. 139, 373–393.

Cottin, J.Y., Lorand, J.P., Agrinier, P., Bodinier, J.L., Liégois, J.P., 1998. Isotopic (O, Sr, Nd) and trace element geochemistry of the Laouni layered intrusions (Pan–African belt, Hoggar, Algeria): evidence for post-collisional continental tholeiitic magmas variably contaminated by continental crust. Lithos 45, 197–222.

Foulger, G.R., Natland, J.H., Anderson, D.L., 2005. A source for Icelandic magmas in remelted Iapetus crust. J. Volcanol. Geotherm. Res. 141, 23–55.

Goldsmith, J.R., 1982. Plagioclase stability at elevated pressures and temperatures. Am. Mineral. 66, 1183–1188.

Govindaraju, K., 1994. Compilation of working values and sample description for 383 geostandards. Geostand. Newsl. 18, 1–158.

Harte, B., Kirkley, M.B., 1997. Partitioning of trace elements between clinopyroxene and garnet: data from mantle eclogites. Chem. Geol. 136, 1–24.

Haüy, M., 1822. Traité de Minéralogie, Seconde édition. Tome deuxième, Bachelier et Huzard, Paris.

Hawkesworth, C.J., Gallagher, K., Hergt, J.M., McDermott, F., 1993. Mantle and slab contributions in arc magmas. Annu. Rev. Earth Planet. Sci. 21, 175–204.

Hermann, J., 2002. Allanite: thorium and light rare earth element carrier in subducted crust. Chem. Geol. 192, 289–306.

Hermann, J., Green, D.H., 2001. Experimental constraints on high pressure melting in subducted crust. Earth Planet. Sci. Lett. 188, 149–168.

Hofmann, A.W., Jochum, K.P., Seufert, M., White, W.M., 1986. Nb and Pb in oceanic basalts: new constraints on mantle evolution. Earth Planet. Sci. Lett. 79, 33–45.

Hoskin, P.W.O., Schaltegger, U., 2003. The composition of zircon and igneous and metamorphic petrogenesis. Rev. Mineral. Geochem. 53, 27–62.

Janák, M., Froitzheim, N., Lupták, B., Vrabec, M., Krogh Ravna, E.J., 2004. First evidence for ultrahigh-pressure metamorphism of eclogites in Pohorje, Slovenia: tracing deep continental subduction in the Eastern Alps. Tectonics 23, TC5014. doi:10.1029/2004TC001641.

Jeffries, T.E., Jackson, S.E., Longerich, H.P., 1998. Application of a frequency quintupled Nd:YAG source (λ=213 nm) for laser ablation ICP-MS analysis of minerals. J. Anal. At. Spectrom. 13, 935–940.

John, T., Schenk, V., 2003. Partial eclogitisation of gabbroic rocks in a late Precambrian subduction zone (Zambia): prograde metamorphism triggered by fluid infiltration. Contrib. Mineral. Petrol. 146, 174–191.

John, T., Scherer, E.E., Haase, K., Schenk, V., 2004. Trace element fractionation during fluid-induced eclogitization in a subducting slab: trace element and Lu–Hf–Sm–Nd isotope systematics. Earth Planet. Sci. Lett. 227, 441–456.

Kelley, K.A., Plank, T., Farr, L., Ludden, J., Staudigel, H., 2005. Subduction recycling of U, Th, and Pb. Earth Planet. Sci. Lett. 234, 369–383.

Kretz, R., 1983. Symbols for rock-forming minerals. Am. Mineral. 68, 277–279.

Krogh Ravna, E.J., 2000. The garnet–clinopyroxene Fe2+–Mg geothermometer: an updated calibration. J. Metamorph. Geol. 18, 211–219.

Krogh Ravna, E.J., Terry, P., 2004. Geothermobarometry of UHP and HP eclogites and schists — an evaluation of equilibria among garnet–clinopyroxene–kyanite–phengite–coesite/quartz. J. Metamorph. Geol. 22, 579–592.

Leake, B.E., Woolley, A.R., Arps, C.E.S., et al., 1997. Nomenclature of amphiboles: report of the subcommittee on amphibole of the International Mineralogical Association, Commission on New Minerals and Mineral Names. Am. Mineral. 82, 1019–1037.

Maury, R.C., Defant, M.J., Joron, J.-L., 1992. Metasomatism of the subarc mantle inferred from trace elements in Philippine xenoliths. Nature 360, 661–663.

Messiga, B., Tribuzio, R., Bottazzi, P., Ottolini, L., 1995. An ion microprobe study on trace element composition of clinopyroxenes from blueschist and eclogitized Fe–Ti-gabbros, Ligurian Alps, northwestern Italy: some petrologic considerations. Geochim. Cosmochim. Acta 59, 59–75.

Michard, P., Gurriet, P., Soudant, N., Albarède, F., 1985. Nd isotopes in French Phanerozoic shales: external vs. internal aspects of crustal evolution. Geochim. Cosmochim. Acta 49, 601–610.

Miller, C., 1990. Petrology of the type locality eclogites from the Koralpe and Saualpe (Eastern Alps), Austria. Schweiz. Mineral. Petrogr. Mitt. 70, 287–300.

Miller, C., Konzett, J., 2005. Comment on "First evidence for ultrahigh-pressure metamorphism of eclogites in Pohorje, Slovenia: tracing deep continental subduction in the eastern Alps" by Marian Janák et al. Tectonics 24, TC6010. doi:10.1029/2004TC001765.

Miller, C., Thöni, M., 1997. Eo-Alpine eclogitisation of Permian MORB-type gabbros in the Koralpe (Austria): new petrological, geochemical and geochronological data. Chem. Geol. 137, 283–310.

Miller, C., Stosch, H.-G., Hoernes, S., 1988. Geochemistry and origin of eclogites from the type locality Koralpe and Saualpe, Eastern Alps, Austria. Chem. Geol. 67, 103–118.

Miller, C., Mundil, R., Thöni, M., Konzett, J., 2005a. Refining the timing of eclogite metamorphism: a geochemical, petrological, Sm–Nd and U–Pb case study from the Pohorje Mountains, Slovenia (Eastern Alps). Contrib. Mineral. Petrol. 150, 70–84.

Miller, C., Thöni, M., Konzett, J., Kurz, W., Schuster, R., 2005b. Eclogites from the Koralpe and Saualpe type-localities, Eastern Alps, Austria. Mitt. Osterr. Mineral. Ges. 150, 227–263.

Mørk, M.B.E., 1985. A gabbro to eclogite transition on Flemsøy, Sunnmore, western Norway. Chem.Geol. 50, 283–310.

Muehlenbachs, K., 1986. Alteration of the oceanic crust and the ^{18}O history of seawater. In: Valley, J.W., Taylor Jr., H.P., O'Neil, J.R. (Eds.), Reviews in Mineralogy. Mineral. Soc. Amer., vol. 16, pp. 424–444.

Nagasaki, A., Enami, M., 1998. Sr-bearing zoisite and epidote in ultra-high pressure (UHP) metamorphic rocks from Su-Lu province, eastern China: an important reservoir under UHP conditions. Am. Mineral. 83, 240–247.

Niu, Y., Batiza, R., 1997. Trace element evidence from seamounts for recycled oceanic crust in the eastern Pacific mantle. Earth Planet. Sci. Lett. 148, 471–483.

Pearce, N.J.G., Perkins, W.T., Westgate, J.A., Gorton, M.P., Jackson, S.E., Neal, C.R., Chenery, S.P., 1997. A compilation of new and published major and trace element data for NIST SRM 610 and NIST SRM 612 glass reference materials. Geostand. Newslett. 21, 115–144.

Powell, R., 1985. Regression diagnostics and robust regression in geothermometer/geobarometer calibration: the garnet–clinopyroxene geothermometer revisited. J. Metamorph. Geol. 3, 231–243.

Ross, K., Elthon, D., 1997. Cumulus and postcumulus crystallization in the oceanic crust: major and trace element geochemistry of Leg 153 gabbroic rocks. Proc. Ocean Drill. Program Sci. Results 153, 333–350.

Rubatto, D., 2002. Zircon trace element geochemistry: partitioning with garnet and the link between U–Pb ages and metamorphism. Chem. Geol. 184, 123–138.

Sassi, R., Harte, B., Carswell, D.A., Yujing, H., 2000. Trace element distribution in Central Dabie eclogites. Contrib. Mineral. Petrol. 139, 298–315.

Sassi, R., Mazzoli, C., Miller, C., Konzett, J., 2004. Geochemistry and metamorphic evolution of the Pohorje Mountain eclogites from the easternmost Austroalpine basement, Eastern Alps, Slovenia. Lithos 78, 235–261.

Scambelluri, M., Philippot, P., 2001. Deep fluids in subduction zones. Lithos 55, 212–227.

Scambelluri, M., Piccardo, G.B., Philippot, P., Robbiano, A., Negretti, L., 1997. High salinity fluid inclusions formed from recycled seawater in deeply subducted alpine serpentinite. Earth Planet. Sci. Lett. 148, 485–500.

Schmidt, M.W., Poli, S., 1998. Experimentally based water budgets for dehydrating slabs and consequences for arc magma generation. Earth Planet. Sci. Lett. 163, 361–379.

Schmidt, M.W., Dardon, A., Chazot, G., Vannucci, R., 2004. The dependence of Nb and Ta rutile–melt partitioning on melt composition and Nb/Ta fractionation during subduction processes. Earth Planet. Sci. Lett. 226, 415–432.

Sölva, H., Grasemann, B., Thöni, M., Thiede, R.C., Habler, G., 2005. The Schneeberg Normal Fault Zone: normal faulting associated with Cretaceous SE-directed extrusion in the Eastern Alps (Italy/Austria). Tectonophysics 401, 143–166.

Spandler, C., Hermann, J., Arculus, R., Mavrogenes, J., 2003. Redistribution of trace elements during prograde metamorphism from lawsonite blueschist to eclogite facies: implications for deep subduction-zone processes. Contrib. Mineral. Petrol. 146, 205–222.

Spandler, C., Hermann, J., Arculus, R., Mavrogenes, J., 2004. Geochemical heterogeneity and element mobility in deeply subducted oceanic crust; insights from high-pressure mafic rocks from New Caledonia. Chem. Geol. 206, 21–42.

Sun, S.S., McDonough, W.F., 1989. Chemical and isotopic systematics of oceanic basalts; implications for mantle composition and processes. In: Saunders, A.D., Norry, M.J. (Eds.), Magmatism in the Oceanic Basins. Spec. Publ. Geol. Soc. Lond., vol. 42, pp. 313–345.

Tiepolo, M., Bottazzi, P., Palenzona, M., Vannucci, R., 2003. A laser probe coupled with ICP-double focusing sector field mass spectrometer for in-situ analysis of trace elements in geological samples and U–Pb dating of zircons. Can. Mineral. 41, 259–272.

Thöni, M., Jagoutz, E., 1992. Some new aspects of dating eclogites in orogenic belts: Sm–Nd, Rb–Sr, and Pb–Pb isotopic results from the Austroalpine Saualpe and Koralpe type-locality (Carinthia/Styria, southeastern Austria). Geochim. Cosmochim. Acta 56, 347–368.

Thöni, M., Miller, C., 1996. Garnet Sm–Nd data from the Saualpe and the Koralpe (Eastern Alps, Austria): chronological and PT constraints on the thermal and tectonic history. J. Metamorph. Geol. 14, 453–466.

Tomascak, P.B., Widom, E., Benton, L.D., Goldstein, S.L., Ryan, J.G., 2002. The control of lithium budgets in island arcs. Earth Planet. Sci. Lett. 196, 227–238.

Tribuzio, R., Messiga, B., Vannucci, R., Bottazzi, P., 1996. Rare earth element redistribution during high-pressure–low-temperature metamorphism in ophiolitic Fe-gabbros (Liguria, northwestern Italy): implications for light REE mobility in subduction zones. Geology 24, 711–714.

Waters, D.J., Martin, H.N., 1993. Geobarometry in phengite-bearing eclogites. Terra Abs. 5, 410–411 (Update%201996: www.earth.ox.ac.uk/~davewa/research/).

Watson, E.B., Wark, D.A., Thomas, J.B., 2006. Crystallization thermometers for zircon and rutile. Contrib. Mineral. Petrol. 151, 413–433.

Wayte, G.J., Worden, R.H., Rubie, D.C., Droop, G.T.R., 1989. A TEM study of disequilibrium plagioclase breakdown at high pressure: the role of infiltrating fluid. Contrib. Mineral. Petrol. 101, 426–437.

Whitehouse, M.J., Platt, J.P., 2003. Dating high-grade metamorphism-constraints from rare-earth elements in zircon and garnet. Contrib. Mineral. Petrol. 145, 61–74.

Woodland, A.B., Seitz, H.-M., Altherr, R., Marschall, H., Olker, B., Ludwig, T., 2002. Li abundances in eclogite minerals: a clue to a crustal or mantle origin? Contrib. Mineral. Petrol. 143, 587–601.

Workman, R.K., Hart, S.R., 2005. Major and trace element composition of the depleted MORB mantle (DMM). Earth Planet. Sci. Lett. 231, 53–72.

Zack, T., Rivers, T., Foley, S.F., 2001. Cs–Rb–Ba systematics in phengite and amphibole: an assessment of fluid mobility at 2.0 GPa in eclogites from Trescolmen, Central Alps. Contrib. Mineral. Petrol. 140, 651–669.

Zack, T., Foley, S.F., Rivers, T., 2002a. Equilibrium and disequilibrium trace element partitioning in hydrous eclogites (Trescolmen, Central Alps). J. Petrol. 43, 1947–1974.

Zack, T., Kronz, A., Foley, S.F., Rivers, T., 2002b. Trace element abundances in rutiles from eclogites and associated garnet mica schists. Chem. Geol. 184, 97–122.

Zack, T., Tomascak, P.B., Rudnick, R.L., Dalpé, C., McDonough, W.F., 2003. Extremely light Li in orogenic eclogites: the role of isotope fractionation during dehydration in subducted oceanic crust. Earth Planet. Sci. Lett. 208, 279–290.

Zack, T., Moraes, R., Kronz, A., 2004. Temperature dependence of Zr in rutile: an empirical calibration of a rutile thermometer. Contrib. Mineral. Petrol. 148, 471–488.

Zhou, M., Robinson, P.T., Lesher, C.M., Keays, R.R., Zhang, C., Malpas, J., 2005. Geochemistry, petrogenesis and metallogenesis of the Panzhihua gabbroic layered intrusion and associated Fe–Ti–V oxide deposits, Sichuan province, SW China. J. Petrol. 46, 2253–2280.